

# 000 TRAIN ON VALIDATION (ToV): 001 002 FAST DATA SELECTION WITH APPLICATIONS TO FINE- 003 TUNING 004

006 **Anonymous authors**

007 Paper under double-blind review

## 010 ABSTRACT

013 State-of-the-art machine learning often follows a two-stage process: *(i)* pre-  
 014 training on large, general-purpose datasets; *(ii)* fine-tuning on task-specific data.  
 015 In fine-tuning, selecting training examples that closely reflect the target distribu-  
 016 tion is crucial. However, it is often the case that only a few samples are available  
 017 from the target distribution. Existing data selection methods treat these target  
 018 samples as a validation set and estimate the effect of adding or removing a single  
 019 sample from the training pool by performing inference on the validation set.

020 We propose a simpler and faster alternative that inverts the usual role of train and  
 021 validation: we perform inference on the training pool before and after fine-tuning  
 022 on the validation set. We then select samples whose predictions change the most.  
 023 Our key insight is that the training samples most affected by fine-tuning on a small  
 024 validation set tend to be the most beneficial for reducing test loss on the target  
 025 distribution. Experiments on instruction tuning and named entity recognition tasks  
 026 show that, in most cases, our method achieves lower test log-loss than state-of-the-  
 027 art approaches. We support our findings with theoretical analysis.

## 028 1 INTRODUCTION

030 While large language models (LLMs) are pretrained on internet-scale datasets, their downstream  
 031 performance can be heavily dependent on the instruction-tuning stage in which they are fine-tuned  
 032 on instruction/output pairs (Ouyang et al., 2022; Zhou et al., 2024; Longpre et al., 2023; Chung  
 033 et al., 2024). These datasets are significantly smaller and are often gathered by using multiple het-  
 034 erogeneous sources. Instruction tuning becomes even more difficult when targeting a specialized use  
 035 case (Wang et al., 2023). More generally, scarcity of domain-specific data is a ubiquitous challenge  
 036 when fine-tuning foundation models.

037 This paper presents an easy-to-implement and low-complexity method for selecting a training  
 038 dataset of prescribed size from heterogeneous sources to maximize the test time performance on  
 039 the target distribution. Our method is motivated by the theory of influence functions (van der Vaart,  
 040 2000) yet avoids the computational burden of computing influence functions. We validate this ap-  
 041 proach on two token-based learning tasks, instruction tuning and named entity recognition (NER),  
 042 and show that in most cases it outperforms state-of-the-art data selection baselines. To illustrate its  
 043 broad applicability, we show that it yields interesting results even for a simple logistic regression  
 044 example (see Appendix D).

045 To formalize the problem, assume access to two datasets: a small dataset from the target distribution  
 046  $\mathbb{P}$  on  $\mathcal{Z}$  and a larger one from possibly heterogeneous data sources. We refer to the dataset from the  
 047 target as the ‘validation set’  $\mathbf{Z}^{\text{val}} := (z_1^{\text{val}}, \dots, z_{m_{\text{val}}}^{\text{val}})$  where  $z_i^{\text{val}}$  are i.i.d. samples from the target  
 048 distribution  $\mathbb{P}$ , and to the larger heterogeneous dataset as ‘training pool’  $\mathbf{X} = (x_1, \dots, x_N)$ , where  
 049  $x_i \in \mathcal{Z}$ . In general the distribution of the training pool differs from  $\mathbb{P}$ . Our goal is to minimize the  
 050 test error on the target distribution with respect to the model parameters  $\theta \in \mathbb{R}^p$ :

$$051 R(\theta) := \mathbb{E}[\ell(\theta, z)], \quad (1)$$

052 where  $\ell : \mathbb{R}^p \times \mathcal{Z} \rightarrow \mathbb{R}$  is a loss function. A separate target-distribution test set  $\mathbf{Z}^{\text{tst}}$  (separate from  
 053  $\mathbf{Z}^{\text{val}}$ ) is used to estimate  $R(\theta)$  after fine-tuning.

We aim to achieve this by training (or fine-tuning) the model on a subset  $S \subseteq [N]$  of the training pool, e.g. running stochastic gradient descent (SGD) with respect to the empirical risk:

$$\hat{R}_S(\boldsymbol{\theta}) := \frac{1}{|S|} \sum_{i \in S} \ell(\boldsymbol{\theta}, \mathbf{x}_i). \quad (2)$$

Let  $\hat{\boldsymbol{\theta}}_S$  be the outcome of running SGD (or any specific training algorithm) on  $\hat{R}_S(\boldsymbol{\theta})$ . We want to select the subset  $S$  (given a constraint on its size  $|S|$ ) so that  $\hat{\boldsymbol{\theta}}_S$  achieves a small test loss on the target distribution, i.e. as to minimize  $R(\hat{\boldsymbol{\theta}}_S)$ .

### 1.1 TRAIN ON VALIDATION: MOTIVATION AND ALGORITHM

To select the most helpful examples at model  $\boldsymbol{\theta}$ , we might score training examples by the decrease in validation loss induced by a single gradient step with respect to that example, then select those with the highest scores. Computing these scores directly requires  $N+1$  full evaluations over the validation set. We derive an efficient approximation to these scores.

Consider a single gradient step with respect to a training example  $\mathbf{x}$ :

$$\boldsymbol{\theta}_{\mathbf{x}} = \boldsymbol{\theta} - \eta \nabla \ell(\boldsymbol{\theta}, \mathbf{x}). \quad (3)$$

The corresponding change in loss for a validation example  $\mathbf{z}$ ,  $\ell(\boldsymbol{\theta}, \mathbf{z}) - \ell(\boldsymbol{\theta}_{\mathbf{x}}, \mathbf{z})$ , can be approximated by a first-order Taylor expansion:

$$\ell(\boldsymbol{\theta}, \mathbf{z}) - \ell(\boldsymbol{\theta}_{\mathbf{x}}, \mathbf{z}) \approx -\langle \nabla \ell(\boldsymbol{\theta}, \mathbf{z}), \boldsymbol{\theta}_{\mathbf{x}} - \boldsymbol{\theta} \rangle = \eta \langle \nabla \ell(\boldsymbol{\theta}, \mathbf{z}), \nabla \ell(\boldsymbol{\theta}, \mathbf{x}) \rangle, \quad (4)$$

where the last step follows from Eq. (3). Pruthi et al. (2020) approximate the scores by computing gradients for each training and validation example and taking their dot products; Xia et al. (2024) extend this to token-based learning. Our method diverges from these approaches: it requires no per-example gradients.

Note the right-hand side is symmetric in  $\mathbf{x}$  and  $\mathbf{z}$ . In other words, the decrease in loss on  $\mathbf{z}$  from a step on  $\mathbf{x}$  is mirrored by the decrease in loss on  $\mathbf{x}$  from a step on  $\mathbf{z}$ . Our method exploits this train-validation symmetry. The change in overall validation loss for a single gradient step with respect to  $\mathbf{x}$  is:

$$\frac{1}{m_{\text{val}}} \sum_{i=1}^{m_{\text{val}}} \left( \ell(\boldsymbol{\theta}, \mathbf{z}_i) - \ell(\boldsymbol{\theta}_{\mathbf{x}}, \mathbf{z}_i) \right) \approx \frac{1}{m_{\text{val}}} \sum_{i=1}^{m_{\text{val}}} \eta \langle \nabla \ell(\boldsymbol{\theta}, \mathbf{z}_i), \nabla \ell(\boldsymbol{\theta}, \mathbf{x}) \rangle. \quad (5)$$

On the other hand, performing a batch gradient step at  $\boldsymbol{\theta}$  with respect to the validation set gives  $\boldsymbol{\theta}_{Z^{\text{val}}} = \boldsymbol{\theta} - \eta \frac{1}{m_{\text{val}}} \sum_{i=1}^{m_{\text{val}}} \nabla \ell(\boldsymbol{\theta}, \mathbf{z}_i)$ . Combining this with Eq. (5), we get

$$\frac{1}{m_{\text{val}}} \sum_{i=1}^{m_{\text{val}}} \left( \ell(\boldsymbol{\theta}, \mathbf{z}_i) - \ell(\boldsymbol{\theta}_{\mathbf{x}}, \mathbf{z}_i) \right) \approx \langle \boldsymbol{\theta} - \boldsymbol{\theta}_{Z^{\text{val}}}, \nabla \ell(\boldsymbol{\theta}, \mathbf{x}) \rangle \approx \ell(\boldsymbol{\theta}, \mathbf{x}) - \ell(\boldsymbol{\theta}_{Z^{\text{val}}}, \mathbf{x}). \quad (6)$$

In other words, the change in average validation loss from training on  $\mathbf{x}$  can be approximated by the change in loss on  $\mathbf{x}$  after training on the validation set  $Z^{\text{val}}$ .

Our main objective is to evaluate the left-hand side of Eq. (6) for all  $\mathbf{x}$  in the training set. The right-hand side provides a far more efficient route: (i) Compute the loss  $\ell(\boldsymbol{\theta}, \mathbf{x})$  for all training examples; (ii) fine-tune  $\boldsymbol{\theta}$  on the validation set to obtain  $\boldsymbol{\theta}_{Z^{\text{val}}}$ ; (iii) re-evaluate the new loss  $\ell(\boldsymbol{\theta}_{Z^{\text{val}}}, \mathbf{x})$  at each training sample  $\mathbf{x}$ , and approximate the effect of training on  $\mathbf{x}$  by computing the difference with the loss at point (i).

This requires one epoch of training on the validation set and two evaluations over the training pool, as opposed to  $N$  evaluations of the validation loss as suggested by a direct evaluation of the left-hand side of Eq. (6), and it does not require access to per-example gradients.

In the next sections we use this idea to obtain a selection algorithm that alternates training on a subset of the training set and on the validation set. A specific implementation, which we refer to as ‘Method A’, is given in Algorithm 1; a slightly different implementation (‘Method B’) will be given in Algorithm 2. In Method A, we start with a small random subset  $U \subset [N]$  of the training pool. We train on  $U$  for  $L$  epochs, resulting in models  $\hat{\boldsymbol{\theta}}_1^{\text{bas}}, \dots, \hat{\boldsymbol{\theta}}_L^{\text{bas}}$ . For each epoch  $k \in [L]$  we fine-tune  $\hat{\boldsymbol{\theta}}_k^{\text{bas}}$  for one epoch on the validation set, resulting in models  $\hat{\boldsymbol{\theta}}_k^{\text{val}}$ . For each epoch, every remaining

---

108 **Algorithm 1** ToV Scoring Algorithm: *Method A*.

---

109  
110 1: **Input:** Pretrained model  $\theta_0$ , validation set  $Z^{\text{val}}$ , training pool  $\mathbf{X} = (\mathbf{x}_i : i \in [N])$ , epochs  $L$ ,  
111 selected data count  $n$ , learning-rate schedule  $\{\eta_k\}_{k=1}^L$ , base model count  $m, \varepsilon \in [0, 1)$   
112 3: **Output:** Set of examples  $S \subset [N]$  of size  $n$   
113 4: Sample base subset  $U \subseteq [N]$  of size  $m$  randomly; define  $\mathbf{X}_U = (\mathbf{x}_i : i \in U)$   
114 5: Initialize model:  $\hat{\theta}_0^{\text{bas}} \leftarrow \theta_0$ ; set scores  $\phi_i \leftarrow 0$  for all  $i \in [N] \setminus U$   
115 6: **for**  $k = 1$  to  $L$  **do**  
116 7:   Train  $\hat{\theta}_{k-1}^{\text{bas}}$  on  $\mathbf{X}_U$  for one epoch with learning rate  $\eta_k$  to obtain  $\hat{\theta}_k^{\text{bas}}$   
117 8:   Train  $\hat{\theta}_k^{\text{bas}}$  for one epoch on  $Z^{\text{val}}$  with a learning rate  $\varepsilon\eta_k$  to obtain  $\hat{\theta}_k^{\text{val}}$   
118 9:   **for** each  $i \in [N] \setminus U$  **do**  
119 10:     $\phi_i^{(k)} \leftarrow F(\ell(\hat{\theta}_k^{\text{val}}; \mathbf{x}_i) - \ell(\hat{\theta}_k^{\text{bas}}; \mathbf{x}_i))$  (see Section 2.1 for the definition of  $F$ )  
120 11:     $\phi_i \leftarrow \phi_i + \phi_i^{(k)}/L$   
121 12:   **end for**  
122 13: **end for**  
123 14: Return set  $S \subseteq [N] \setminus U$  of size  $n$  on the basis of scores  $\phi_i$  (see text)

---

124  
125

126 training example  $\mathbf{x}_i$  with  $i \in [N] \setminus U$  is scored by the change in its loss between  $\hat{\theta}_k^{\text{bas}}$  and  $\hat{\theta}_k^{\text{val}}$ , and  
127 scores are averaged across epochs.

128 After computing scores  $\phi_i$  as in Algorithm 1, we select  $S$  using one of two strategies: (i) choose  
129 the  $n$  examples with the largest  $\phi_i$ ; (ii) choose half from the highest-scoring examples and the other  
130 half uniformly at random from  $U$  to increase diversity.

132 Intuitively, large  $\phi_i$  means that a small amount of training on the target distribution produces a large  
133 change in the model output at  $\mathbf{x}_i$ . Our working assumption, motivated by the heuristics above and  
134 formalized in Section 3, is that the converse also holds: training on  $\mathbf{x}_i$  will produce a large change  
135 in model output on the target distribution. Hence the scores  $\phi_i$  can be used to select ‘important’  
136 samples for the target.

137 An adaptation for token-based learning is described in Section 2, along with empirical results. Section 3  
138 provides a mathematical justification that formalizes the argument above.

140 1.2 RELATED WORK

143 Our work relates to data selection and data attribution. The impact of a single example on the  
144 validation error can be approximated by a first-order Taylor expansion. This idea results in data  
145 selection methods based on influence functions (Wang et al., 2018; 2020; Ai et al., 2021; Kolosov  
146 et al., 2024). Classical influence functions estimate the effect of a single example on the empirical  
147 risk minimizer. Most closely related to our work are Pruthi et al. (2020); Bae et al. (2024); Xia et al.  
148 (2024), which instead estimate the influence of an example on the training dynamics. In particular,  
149 Bae et al. (2024) shows how to approximately propagate gradient changes at  $k$ -th epoch through all  
150 subsequent epochs. In contrast, Pruthi et al. (2020); Xia et al. (2024) make a crude approximation  
151 for this propagation. Limitations of influence-based methods are discussed in Schioppa et al. (2023).

152 The recent work of Xia et al. (2024) proposes LESS, a data selection method for instruction tuning  
153 that adapts influence ideas to Adam and long sequences. In particular, these authors emphasize the  
154 challenge of computing and storing gradients to compute influences. They address this problem  
155 via random projections and low-rank approximation. Engstrom et al. (2024) apply the datamodel  
156 framework (Ilyas et al., 2022; Park et al., 2023) to select pretraining data. Separately, a *replay*  
157 algorithm that stores only a logarithmic number of checkpoints is proposed in Engstrom et al. (2025).  
158 Methods that align training data distributions to a small target set include TSDS (Liu et al., 2024) and  
159 DSIR (Xie et al., 2023); domain/task-adaptive pretraining also improves transfer (Gururangan et al.,  
160 2020). Broader LLM data-efficiency work proposes LLM-guided quality scoring (Ask-LLM) and  
161 density sampling (Sachdeva et al., 2024), and clustering-based sensitivity sampling with provable  
162 guarantees (Axiotis et al., 2024). Finally, Data Filtering Networks (DFN) also leverage a held-out,  
163 high-quality set, but with a different goal and setup (Fang et al., 2023).

162 Our contribution differs by (i) inverting train/validation roles to approximate per-example influence  
 163 using only forward losses and doesn't require per example gradients, or Hessian-vector products—and (ii) showing that this simple, symmetry-based score is computationally inexpensive and  
 164 outperforms recent data selection approaches for instruction tuning and NER.  
 165

## 167 2 DATA SELECTION FOR TOKEN-BASED LEARNING

169 In this section we describe our implementation of the general idea described in the introduction  
 170 for token-based learning and present empirical results demonstrating its effectiveness. Since pre-  
 171 diction takes place at the token level, while data selection takes place at the example level (e.g.,  
 172 instruction/output pair), we compute token scores and aggregate them as described in Section 2.1.  
 173 Section 2.2 gives a brief overview of instruction-tuning and NER tasks. Experimental settings are  
 174 introduced in Section 2.3. Empirical results are presented in Sections 2.4 and 2.5.  
 175

### 176 2.1 SCORE COMPUTATION FOR TOKEN-BASED LEARNING

178 Each example  $z$  consists of an input  $z^{\text{in}}$  and an output  $z^{\text{out}}$ , both of which are strings and may differ  
 179 in length. Let  $\mathcal{Z}^{\text{out}}$  denote the output vocabulary, and let  $T(z)$  denote the length of the output string  
 180  $z^{\text{out}}$ , which we write as  $z^{\text{out}} = (z^{\text{out}}(1), z^{\text{out}}(2), \dots, z^{\text{out}}(T(z)))$ .

181 Given a model parameterized by  $\theta$ , its prediction on example  $z$  is a sequence of  $T(z)$  conditional  
 182 distributions,  $\{p_t(\cdot | z, \theta)\}_{t=1}^{T(z)}$ , where each  $p_t(\cdot | z, \theta)$  denotes the model's predictive distribution  
 183 over the output token at position  $t$ . Note that  $p_t(\cdot | z, \theta)$  depends on  $z$  solely through  $z^{\text{in}}$  and  
 184  $z^{\text{out}}(1), \dots, z^{\text{out}}(t-1)$ . We train models using the log-loss  
 185

$$186 \ell(\theta; z) = -\frac{1}{T(z)} \sum_{t=1}^{T(z)} \log p_t(z^{\text{out}}(t) | z; \theta). \quad (7)$$

187 To compare two models,  $\theta$  and  $\theta'$ , on example  $z$ , we define a per-token difference of log-loss  
 188

$$189 \Delta_t(z; \theta, \theta') = \log \frac{p_t(z^{\text{out}}(t) | z; \theta')}{p_t(z^{\text{out}}(t) | z; \theta)}. \quad (8)$$

192 Since our setting involves selecting entire examples rather than individual tokens, we aggregate  
 193 the per-token differences into a single score per example. Specifically, we apply a transformation  
 194 function  $F : \mathbb{R} \rightarrow \mathbb{R}$  to each  $\Delta_t$  before averaging across positions. The final score for example  $z$  is:  
 195

$$196 \phi(z; \theta, \theta') = \frac{1}{T(z)} \sum_{t=1}^{T(z)} F(\Delta_t(z; \theta, \theta')). \quad (9)$$

198 We consider three instantiations of the function  $F$ , leading to three different scoring methods:

199 **MAXIMUM-IMPROVEMENT:**  $F(y) = y$  — emphasizes raw improvement.

201 **MAXIMUM-ABSOLUTE CHANGE:**  $F(y) = |y|$  — captures the magnitude of change.

202 **MAXIMUM-POSITIVE IMPROVEMENT:**  $F(y) = \max\{y, 0\}$  — ignores degradations.

204 The algorithm is therefore the same as in Algorithm 1, with the adaptation  $\phi_i^{(k)} = \phi(\mathbf{x}_i; \hat{\theta}_k^{\text{bas}}, \hat{\theta}_k^{\text{val}})$ .  
 205

206 Given a budget of  $n$  examples, we choose  $S \subseteq [N] \setminus U$ ,  $|S| = n$  using one of these rules:

207 **SCORE-ONLY:** Choose the  $n$  examples  $i \in [N] \setminus U$  that have the largest score  $\phi_i$ .

208 **SCORE+RANDOM:** Choose the  $n/2$  examples  $i \in [N] \setminus U$  that have the largest score  $\phi_i$ , and add  
 209  $n/2$  more examples chosen uniformly at random (without replacement) from  $U$ .

211 Our scoring schemes tend to favor shorter examples due to their higher variance, which arises from  
 212 having fewer tokens. To mitigate this bias, we partition the set  $[N] \setminus U$  into 10 bins based on sequence  
 213 length, ensuring each bin contains an equal number of examples. We then select an equal number of  
 214 top-scoring examples from each bin.

215 After selecting  $S$  of size  $|S| = n$ , we train (or fine tune) a model on  $S$  to evaluate the selection  
 scheme. We refer to this stage as *final training*.

216 We compare our schemes with three baselines:  
 217  
 218 **RANDOM**: The set  $S$  is selected uniformly at random subject to its size.  
 219  
 220 **MAXIMUM UNCERTAINTY**: Instead of the scores we defined, we use the following hardness score:  
 221  
 222
 
$$\psi_i := \frac{1}{T_i} \sum_{t=1}^{T_i} \log (p_t(z_i(t)|z_i; \hat{\theta}_L^{\text{bas}})(1 - p_t(z_i(t)|z_i; \hat{\theta}_L^{\text{bas}}))), \quad (10)$$
 223 This score extends the method of [Ting & Brochu \(2018\)](#); [Wang et al. \(2018\)](#); [Ai et al. \(2021\)](#);  
 224 [Kolossov et al. \(2024\)](#) to token-based learning .  
 225  
 226 **LESS**: We used the publicly available implementation from [Xia et al. \(2024\)](#); see Appendix A.1.

## 227 2.2 PREDICTION TASKS

228 We evaluate our data selection framework in two distinct token-based tasks: instruction tuning (IT)  
 229 and named entity recognition (NER). The framework we introduced above captures both tasks:

231 **Instruction Tuning (IT)** involves training a language model to follow natural language instructions.  
 232 Each training example consists of:

233 **Input**  $z^{\text{in}}$ : a user instruction or prompt; **Output**  $z^{\text{out}}$ : the desired model response.

234 The output is typically multi-token and highly variable in content and length, depending on the  
 235 instruction. The model learns to generate  $z^{\text{out}}$  conditioned on  $z^{\text{in}}$ . This naturally fits our framework,  
 236 which models predictions as token-level distributions  $p_t(\cdot | z, \theta)$ .

237 **Named Entity Recognition (NER)** is a sequence labeling task where the model assigns a probabil-  
 238 ity distribution over entity tags (e.g., PERSON, ORGANIZATION, ...) to each token. In this case:  
 239 **Input**  $z^{\text{in}}$ : a tokenized sentence; **Output**  $z^{\text{out}}$ : a sequence of entity labels, aligned with the input.

241 In NER, predictions are computed as token-wise classification distributions and therefore output is  
 242 of the same length as input sequence.<sup>1</sup> In this case, as a base model we take a pretrained language  
 243 model and replace its prediction head with a classification head.

## 245 2.3 EXPERIMENTAL SETTING

247 In all of our experiments the training set consisted of  $N = 36 \times 1024$  samples. For the base model  
 248 training, we used  $|U| = 4 \times 1024$  samples. The validation set size is  $m_{\text{val}} = 1024$  and the test set  
 249 size is  $m_{\text{test}} = 10,000$ . We vary the selected set size  $n \in \{1, 2, 4, 8\} \times 1024$ .

250 **Number of epochs.** Both for surrogate model training and final model training we determine the  
 251 number of epochs by  $L = (16 \times 1024)/n_{\text{tr}}$ . We use a batch size of 16 whence the above ensures  
 252 that the number batches used in training remains constant, and equal to 1024. In other words, all  
 253 experiments in this section are at *constant compute*. Since base model training uses  $|U| = m =$   
 254  $4 \times 1024$  samples, the number of epochs is  $L = 4$ .

255 **Learning rate.** The learning rate for both surrogate and final model training is selected using hyper-  
 256 parameter optimization for each selected set size  $n$ . The learning-rate optimization was carried out  
 257 for random data selection hence placing our approach at a disadvantage.

258 We use linear learning rate scheduler and LoRA training [Hu et al. \(2022\)](#) with LoRA parameters  
 259  $\alpha = 32$  and  $\text{dropout} = 0.2$ . For NER experiments, we used PEFTrank = 1 and for instruction  
 260 tuning experiments, we used PEFTrank = 256. The learning rate for the validation examples is  
 261  $\varepsilon = 1/10$  of the one for the base examples. We present here results with SCORE+RANDOM and  
 262 refer to the appendix for SCORE-ONLY.

## 264 2.4 EXPERIMENTS FOR INSTRUCTION TUNING

266 For these experiments we used 3 different datasets, which we will refer to as  $\mathcal{S} := \{\text{Slim Orca},$   
 267  $\text{Alpaca GPT-4}, \text{Alpaca GPT-3.5}\}$ . As the foundation model, we use **Meta-Llama-3-8B**. Additional  
 268 details of the model and datasets used are provided in the Appendix.

269 <sup>1</sup>In NER, typically token level probabilities are combined to assign labels to a whole word.

We designed five experimental setups. In each experiment, one dataset from  $\mathcal{S}$  is selected as the *target distribution*. We randomly sample validation and test sets,  $Z^{\text{val}}$  and  $Z^{\text{test}}$ , without replacement from the target dataset. These samples are excluded from further use. The *training pool* is then formed by randomly sampling an equal number of examples from one or more datasets in  $\mathcal{S}$  (excluding the validation and test samples), such that the total number of selected training samples is fixed at  $N$ . We denote by  $\mathcal{S}_* \subseteq \mathcal{S}$  the datasets used to generate the training pool. The choices of the target dataset and of  $\mathcal{S}_*$  for each of the five experiments are summarized in Table 1. All reported results are averaged over 10 independent runs. In each run, we freshly sample the training, validation, and test sets. These experiments are designed to evaluate performance across a range of data configurations. In particular: in Experiments 1 and 4, the training set includes samples from both target distribution and other distributions; in Experiments 2 and 5, the training set includes samples only from non-target distributions; in Experiment 3, it includes only samples from the target distribution.

Table 1: Summary of instruction tuning experiments. Abbreviations: SO = Slim Orca, A4 = Alpaca GPT-4, A3.5 = Alpaca GPT-3.5.

Exp	Target	Training pool
1	SO	SO, A4, and A3.5
2	SO	A4 and A3.5
3	SO	SO
4	A4	SO, A4, and A3.5
5	A4	SO and A3.5

Table 2: Summary of named entity recognition experiments. Abbreviations: MN = Multinerd, A4p = Ai4p, C4 = C4, SB = Syn-big.

Exp	Target	Training pool
1	MN	MN, A4p, C4, and SB
2	MN	A4p, C4, and SB
3	MN	MN
4	A4p	MN, A4p, C4, and SB
5	A4p	MN, C4, and SB
6	A4p	A4p

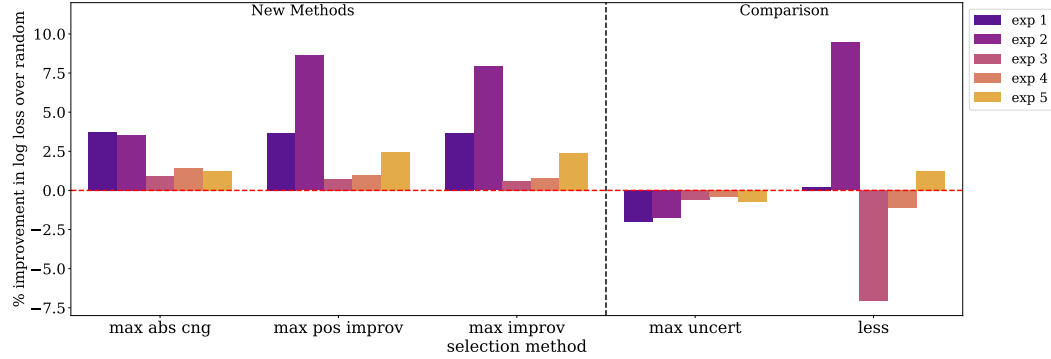


Figure 1: Test log-loss improvement (%) over random selection for instruction tuning with  $n = 8 \times 1024$  samples. Each group of bars represents a data-selection strategy (maximum-uncertainty and LESS as baselines); colors show target/training pool configuration (Table 1). Results use Method A (Algorithm 1) with the SCORE+RANDOM strategy.

Figure 1 summarizes our results for instruction tuning for a fixed select size  $n = 8 \times 1024$ . We plot the improvement in test log-loss over random data selection for several data-selection strategies within the general framework described in Section 2.1, using method A in algorithm 1 for scoring the examples and SCORE+RANDOM for selecting. We observe that the proposed strategies yield significantly better instruction tuning than random data selection or selecting by max-uncertainty. We observe an improvement (albeit a small one) even when both train and validation data are from Slim Orca (Exp 3), which is a case in which random selection should perform well. The proposed strategies also yield a significant improvement over LESS (Xia et al., 2024), with the exception of Experiment 2 in which LESS performs slightly better.

Figure 2 displays the evolution of test log loss with selected sample size  $n$ . We observe that a good choice of the data selection method results in model improvements that can be equivalent to or larger than doubling  $n$ . Plots show standard error (with scaling factor 1) for 10 runs.

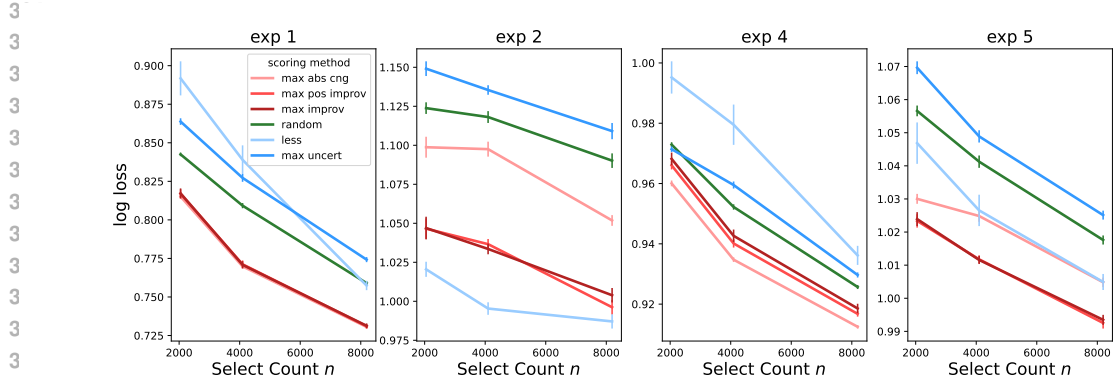


Figure 2: Test log-loss vs. number of selected samples  $n$  for instruction tuning. (Due to space limits, Exp. 3 plot is in the Appendix.) Lines show mean log-loss over 10 runs; error bars are  $\pm 1$  standard error. Results use Method A with the SCORE+RANDOM strategy.

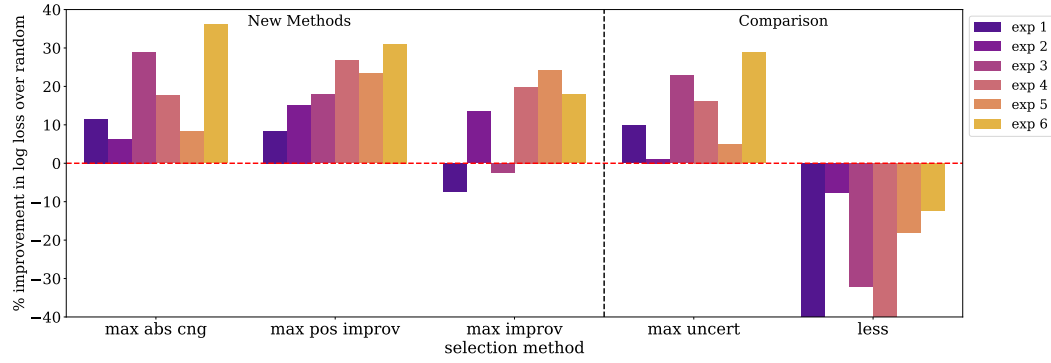


Figure 3: Test log-loss improvement (%) relative to random selection for NER at  $n = 8 \times 1024$ . Each group of bars represents a data-selection strategy; colors show target/training pool configuration (Table 2). Results use Method A (Algorithm 1) with the SCORE+RANDOM strategy

## 2.5 EXPERIMENTS FOR NAMED ENTITY RECOGNITION

The task is to classify whether a token is part of a person name or not. For these experiments we used 4 different labeled datasets, which we will refer to as  $\mathcal{S} := \{ \text{Multinerd}, \text{Ai4p}, \text{C4}, \text{Syn-big} \}$ . We use **xlm-roberta-base** as the foundation model. Further details on the experiment, model and datasets used are presented in the Appendix.

We conducted six sets of experiments. As for the case of instruction tuning, for each set of experiments, we select one of the datasets  $\mathcal{S}$  as defining the target distribution, and one or more other datasets to define the training pool (denoted by  $\mathcal{S}_*$ ). The choices of target datasets and  $\mathcal{S}_*$  are summarized in Table 2. The construction of train, test and validation sets is same as in instruction tuning.

Figure 3 summarizes our experiments with NER. We plot the improvement in test log-loss over random data selection for several scores definitions. Throughout these experiments, we use SCORE+RANDOM. We observe that the strategies of Section 2.1 yield systematic improvements over random data-selection. Unlike in the case of instruction tuning, maximum uncertainty also yields an improvement in most settings. However, the ToV approach achieves a larger improvement. Finally, in this case LESS (Xia et al., 2024) appears not to improve over random data selection.

## 3 A FORMAL JUSTIFICATION

In this section we present a mathematical analysis of our approach in the case of batch gradient descent (GD). We focus on the implementation *Method B*, described in Algorithm 2.

---

378 **Algorithm 2** ToV Scoring Algorithm: *Method B*

---

```

380 1: Input: Pretrained model  $\theta_0$ , validation set  $Z^{\text{val}}$ , training pool  $\mathbf{X} = (\mathbf{x}_i : i \in [N])$ ,
381 2:           selected data count  $n \leq N$ , base model count  $m$ 
382 3: Output: Set of examples  $S \subset [N]$  of size  $n$ 
383 4: Sample base subset  $U \subseteq [N]$  of size  $m$  randomly; define  $\mathbf{X}_U = (\mathbf{x}_i : i \in U)$ 
384 5: Initialize models:  $\hat{\theta}_0^{\text{bas},+} \leftarrow \theta_0$ ,  $\hat{\theta}_0^{\text{bas}} \leftarrow \theta_0$ ; set scores  $\Upsilon_i \leftarrow 0$  for all  $i \in [N] \setminus U$ 
385 6: for  $k = 1$  to  $L$  do
386 7:   Train for one epoch on  $\mathbf{X}_U$  with learn. rate  $\eta_k$  and init.  $\hat{\theta}_{k-1}^{\text{bas},+}$ . Denote the output by  $\hat{\theta}_{0,k}^{\text{bas},+}$ 
387 8:   Train for one epoch on  $Z^{\text{val}}$  with learn. rate  $\varepsilon \cdot \eta_k$  and init.  $\hat{\theta}_{0,k}^{\text{bas},+}$ . Denote the output by  $\hat{\theta}_k^{\text{bas},+}$ 
388 9:   Train for one epoch on  $\mathbf{X}_U$  with learn. rate  $\eta_k$  and init.  $\hat{\theta}_{k-1}^{\text{bas}}$ . Denote the output by  $\hat{\theta}_k^{\text{bas}}$ 
389 10:  for each  $i \in [N] \setminus U$  do
390 11:     $\Upsilon_i^{(k)} \leftarrow \ell(\hat{\theta}_k^{\text{bas}}; \mathbf{x}_i) - \ell(\hat{\theta}_k^{\text{bas},+}; \mathbf{x}_i)$ 
391 12:     $\Upsilon_i \leftarrow \Upsilon_i + \Upsilon_i^{(k)}/L$ 
392 13:  end for
393 14: end for
394 15: Select  $S \subseteq [N] \setminus U$  with size  $|S| = n$  using scores  $\Upsilon_i$ 
395
396
```

---

397 Method B differs from Method A because at each training cycle  $k$ , training on the base set  $\mathbf{X}_U$  is  
398 initialized with the output of the previous train-on-validation phase. Empirically Method A performs  
399 somewhat better than B, see Appendix C. We use Method B for analysis just because the resulting  
400 mathematical expressions are simpler.

401 We find empirically that the ToV works well beyond token-based learning, and hence our focus  
402 will be to understand it in a generic learning problem. Appendix D demonstrates this point by  
403 considering a simple logistic regression problem.  
404

### 405 3.1 IDEAL SCORES, LINEARIZATION, INFLUENCE FUNCTIONS

406 In order to estimate the model improvement produced by sample  $i \in [N] \setminus U$  we could train a model  
407 on two training sets  $\mathbf{X}_U$  and  $\mathbf{X}_{U \cup i}$ , using empirical risk functions  $\hat{R}_U(\theta)$ ,  $\hat{R}_{U \cup i}(\theta)$ . We thus would  
408 run GD for  $L$  steps, with initialization  $\hat{\theta}_0^{\text{bas}} = \hat{\theta}_0^{\text{bas}+i} = \theta_0$ :

$$410 \quad \hat{\theta}_{k+1}^{\text{bas}} = \hat{\theta}_k^{\text{bas}} - \eta m \nabla \hat{R}_U(\hat{\theta}_k^{\text{bas}}), \quad \hat{\theta}_{k+1}^{\text{bas}+i} = \hat{\theta}_k^{\text{bas}+i} - \eta(m+1) \nabla \hat{R}_{U \cup i}(\hat{\theta}_k^{\text{bas}+i}). \quad (11)$$

411 At iteration  $k$ , we have thus two models  $\hat{\theta}_k^{\text{bas}}$  and  $\hat{\theta}_k^{\text{bas}+i}$  that differ uniquely in whether sample  $i$  is  
412 used or not. We define the *ideal score* to be the difference in validation error between these two  
413 models, averaged over epochs

$$414 \quad S_i := \frac{1}{L} \sum_{s=1}^L [\hat{R}_{\text{val}}(\hat{\theta}_s^{\text{bas}}) - \hat{R}_{\text{val}}(\hat{\theta}_s^{\text{bas}+i})] = \frac{1}{m_{\text{val}} L} \sum_{s=1}^L \sum_{j=1}^{m_{\text{val}}} \{ \ell(\hat{\theta}_s^{\text{bas}}; \mathbf{z}_j^{\text{val}}) - \ell(\hat{\theta}_s^{\text{bas}+i}; \mathbf{z}_j^{\text{val}}) \}. \quad (12)$$

415 Evaluating this score is computationally expensive, hence several groups (Pruthi et al., 2020; Bae  
416 et al., 2024; Xia et al., 2024) proposed to use a first order Taylor expansion to approximate the  
417 difference between the two models. Expanding  $S_i$  with respect to the contribution of  $\ell(\cdot; \mathbf{x}_i)$  yields

$$418 \quad S_i^{\text{lin}} = \frac{\eta}{L} \sum_{0 \leq s < t \leq L} \langle \nabla \hat{R}_{\text{val}}(\hat{\theta}_t^{\text{bas}}), \mathbf{M}_{t,s+1} \nabla \ell(\hat{\theta}_s^{\text{bas}}; \mathbf{x}_i) \rangle. \quad (13)$$

419 where  $\mathbf{M}_{t,t} = \mathbf{I}_d$  and  $\mathbf{M}_{t,r}$  captures the propagation of perturbations along the GD trajectory:  
420

$$421 \quad \mathbf{M}_{t,r} := \mathbf{H}_{t-1} \cdot \mathbf{H}_{t-2} \cdots \mathbf{H}_r, \quad \mathbf{H}_k := \mathbf{I} - \eta m \nabla^2 \hat{R}_U(\hat{\theta}_k^{\text{bas}}). \quad (14)$$

422 The next result shows that  $S_i^{\text{lin}}$  approximates well  $S_i$  in a quantitative way, under local convexity.

423 **Proposition 1.** *Assume there exist  $c_0, C_1, M > 0$  such that  $\nabla^2 \hat{R}_U(\hat{\theta}_k^{\text{bas}}) \succeq c_0 \mathbf{I}_d$ ,  $\|\nabla \ell(\hat{\theta}_k^{\text{bas}}; \mathbf{x}_i)\| \leq$   
424  $C_1$  for all  $k$  and, for all  $\theta_1, \theta_2$ ,  $\|\nabla^2 \hat{R}_U(\theta_1) - \nabla^2 \hat{R}_U(\theta_2)\|_{\text{op}} \leq M \|\theta_1 - \theta_2\|_2$ ,  $\|\nabla \ell(\theta_1; \mathbf{x}_i) -$   
425  $\nabla \ell(\theta_2; \mathbf{x}_i)\|_{\text{op}} \leq M \|\theta_1 - \theta_2\|_2$ . Further assume that  $\|\nabla^2 \hat{R}_{\text{val}}(\hat{\theta}_k^{\text{bas}})\|_{\text{op}} \leq C_1$  and  $\|\nabla^2 \hat{R}_{\text{val}}(\theta_1) -$*

432  $\nabla^2 \widehat{R}_{\text{val}}(\boldsymbol{\theta}_2) \|_{\text{op}} \leq M \|\boldsymbol{\theta}_1 - \boldsymbol{\theta}_2\|_2$  for all  $\boldsymbol{\theta}_1, \boldsymbol{\theta}_2$  as well. Finally, assume there exists a constant  $C_\eta$   
 433 such that  $\eta_k = \eta \leq C_\eta/m \forall k$ . Then there exists  $C = C(c_0, C_1, C_\eta, M)$  such that

$$434 \quad 435 \quad |S_i - S_i^{\text{lin}}| \leq C/m^2. \quad (15)$$

436 The assumption  $\eta \leq C_\eta/m$  is justified by the fact that we expect the Hessian of  $\widehat{R}_U(\cdot)$  to be of  
 437 order one, and hence the stepsize for this objective (which is given by  $\eta m$  see Eq. (11)) should be  
 438 of order one. As shown in the proof, the typical size of  $S_i^{\text{lin}}$  is of order  $1/m$ , and hence Eq. (15)  
 439 establishes that the difference  $|S_i - S_i^{\text{lin}}|$  is negligible.  
 440

### 441 3.2 TRAIN-VALIDATION DUALITY

443 We consider Methods A and B defined in Algorithms 1, 2. We emphasize the dependence on  $\varepsilon$  by  
 444 writing  $\phi_i = \phi_i(\varepsilon)$  and  $\Upsilon_i = \Upsilon_i(\varepsilon)$ . It is easy to derive the small  $\varepsilon$  asymptotics  $\phi_i = \phi_i^{\text{lin}} \varepsilon + o(\varepsilon)$ ,  
 445  $\Upsilon_i = \Upsilon_i^{\text{lin}} \varepsilon + o(\varepsilon)$ , where, for  $\mathbf{g}_{s,i} := \nabla \ell(\hat{\boldsymbol{\theta}}_s^{\text{bas}}; \mathbf{x}_i)$ ,

$$446 \quad 447 \quad \phi_i^{\text{lin}} := \frac{\eta m_{\text{val}}}{L} \sum_{s=1}^L \langle \nabla \widehat{R}_{\text{val}}(\hat{\boldsymbol{\theta}}_s^{\text{bas}}), \mathbf{g}_{s,i} \rangle, \quad \Upsilon_i^{\text{lin}} := \frac{\eta m_{\text{val}}}{L} \sum_{0 \leq t < s \leq L} \langle \nabla \widehat{R}_{\text{val}}(\hat{\boldsymbol{\theta}}_{t+1}^{\text{bas}}), \mathbf{M}_{s,t+1}^{\text{T}} \mathbf{g}_{s,i} \rangle. \quad (16)$$

449 We show that these are good approximations of  $\Upsilon_i(\varepsilon), \phi_i(\varepsilon)$  uniformly in dimension, sample size.  
 450

451 **Theorem 1.** Consider Algorithms 1, 2 with fixed stepsize  $\eta_k = \eta$  (and  $F(x) = -x$  in Algorithm  
 452 1). Under the assumptions of Proposition 1, further assume  $\|\nabla \widehat{R}_{\text{val}}(\hat{\boldsymbol{\theta}}_k^{\text{bas}})\| \leq C_1$  for all  $k$ , and  
 453  $\|\nabla^2 \ell(\boldsymbol{\theta}; \mathbf{x})\|_{\text{op}} \leq C_1$ . Then there exist  $c_* = c_*(c_0, M, C_1)$ ,  $C = C(c_0, M, C_1)$  such that, for  
 454  $\varepsilon m_{\text{val}}/m \leq c_*$ ,

$$455 \quad |\Upsilon_i(\varepsilon) - \Upsilon_i^{\text{lin}} \varepsilon| \leq C(\varepsilon m_{\text{val}}/m)^2, \quad |\phi_i(\varepsilon) - \phi_i^{\text{lin}} \varepsilon| \leq C(\varepsilon m_{\text{val}}/m)^2. \quad (17)$$

456 Note that  $\Upsilon_i^{\text{lin}}$  differ from  $S_i^{\text{lin}}$  because of: (i) The different order of  $s$  and  $t$ ; (ii) The fact that  $\mathbf{M}_{t,s+1}$   
 457 is replaced by its transpose in Eq. (16).  $\Upsilon_i^{\text{lin}}$  measures the influence of training on validation data  
 458 when making inference at  $\mathbf{x}_i$ , while  $S_i^{\text{lin}}$  measures the influence of training on  $\mathbf{x}_i$  data when making  
 459 inference on validation. These two measures of ‘influence’ differ by the replacement of  $\mathbf{M}_{t,s+1}$  by  
 460  $\mathbf{M}_{s,t}^{\text{T}}$ . However, in a number of cases we expect these two matrices to be not too different, and hence  
 461 the two scores to yield similar results. We can prove that  $\Upsilon_i^{\text{lin}}$  and  $S_i^{\text{lin}}$  coincide (for large  $L$ ) under  
 462 local convexity conditions.  
 463

464 **Theorem 2.** Assume  $\boldsymbol{\theta} \mapsto \ell(\boldsymbol{\theta}; \mathbf{x})$  to be twice continuously differentiable and that  $\|\nabla \widehat{R}_{\text{val}}(\hat{\boldsymbol{\theta}}_k^{\text{bas}})\| \leq$   
 465  $C_1$ ,  $\|\nabla \ell(\hat{\boldsymbol{\theta}}_k^{\text{bas}}; \mathbf{x}_i)\| \leq C_1$  for all  $k$ . Further assume that gradient descent iterates  $(\hat{\boldsymbol{\theta}}_k^{\text{bas}} : k \geq 0)$   
 466 converge to  $\hat{\boldsymbol{\theta}}_\infty^{\text{bas}} = \lim_{k \rightarrow \infty} \hat{\boldsymbol{\theta}}_k^{\text{bas}}$  which is a local minimum of  $\widehat{R}_U(\boldsymbol{\theta})$  with  $\mathbf{Q}_\infty := \nabla^2 \widehat{R}_U(\hat{\boldsymbol{\theta}}_\infty^{\text{bas}}) \succ \mathbf{0}$   
 467 (strictly). Then

$$468 \quad 469 \quad \lim_{L \rightarrow \infty} \frac{1}{m_{\text{val}}} \Upsilon_i^{\text{lin}}(L) = \lim_{L \rightarrow \infty} S_i^{\text{lin}}(L) = \frac{1}{m} \langle \nabla \widehat{R}_{\text{val}}(\hat{\boldsymbol{\theta}}_\infty^{\text{bas}}), \mathbf{Q}_\infty^{-1} \nabla \ell(\hat{\boldsymbol{\theta}}_\infty^{\text{bas}}; \mathbf{x}_i) \rangle := S_{i,\infty}^{\text{lin}}. \quad (18)$$

470 The last expression in Eq. (18) (denoted by  $S_{i,\infty}^{\text{lin}}$ ) is the classical formula for influence functions of  
 471 M-estimators (van der Vaart, 2000). Both our approach and the dynamical influence function  $S_i^{\text{lin}}(L)$   
 472 can be regarded as approximations of  $S_{i,\infty}^{\text{lin}}$  in this case.  
 473

474 In fine tuning, the model is likely to be overparametrized, and it is unrealistic to assume convergence  
 475 to a strict minimum (with  $\nabla^2 \widehat{R}_U(\hat{\boldsymbol{\theta}}_\infty^{\text{bas}}) \succ \mathbf{0}$ ). On the other hand, the weights will not change signifi-  
 476 cantly during this phase and it is reasonable to approximate fine-tuning as fitting an overparametrized  
 477 linear model with respect to the empirical neural tangent features learnt in the pre-training phase.

478 **Theorem 3.** Consider the loss function  $\ell(\boldsymbol{\theta}; \mathbf{x}) = (y(\mathbf{x}) - \langle \boldsymbol{\psi}(\mathbf{x}), \boldsymbol{\theta} \rangle)^2/2$  for some response vari-  
 479 ables  $y(\mathbf{x})$ , and featurization map  $\boldsymbol{\psi} : \mathbb{R}^d \rightarrow \mathbb{R}^p$ ,  $p > m$ . Let  $\boldsymbol{\Psi} \in \mathbb{R}^{|U| \times p}$  be the matrix with rows  
 480  $(\boldsymbol{\psi}(\mathbf{x}_j) : j \in U)$ ,  $\boldsymbol{\Psi}_{\text{val}} \in \mathbb{R}^{m_{\text{val}} \times p}$  be the matrix with rows  $(\boldsymbol{\psi}(\mathbf{z}_j^{\text{val}}) : j \leq m_{\text{val}})$ ,  $\mathbf{P}_\Psi$  the projector to  
 481 the kernel of  $\boldsymbol{\Psi}$ ,  $\mathbf{y} = (y(\mathbf{x}_j) : j \in U)$ ,  $\hat{\boldsymbol{\theta}} := \boldsymbol{\Psi}^\dagger \mathbf{y}$ ,  $\mathbf{r}^{\text{val}} := (y(\mathbf{z}_j^{\text{val}}) - \langle \hat{\boldsymbol{\theta}}, \boldsymbol{\psi}(\mathbf{z}_j^{\text{val}}) \rangle : j \leq m_{\text{val}})$ ,  
 482  $r(i) := y(\mathbf{x}_i) - \langle \hat{\boldsymbol{\theta}}, \boldsymbol{\psi}(\mathbf{x}_i) \rangle$ . If GD is initialized with  $\boldsymbol{\theta}_0 = \mathbf{0}$ , and we use constant stepsize  
 483  $\eta < \|\boldsymbol{\Psi}\|_{\text{op}}^2/2$ , then

$$484 \quad 485 \quad \lim_{L \rightarrow \infty} \frac{1}{L m_{\text{val}}} \Upsilon_i^{\text{lin}}(L) = \lim_{L \rightarrow \infty} \frac{1}{L} S_i^{\text{lin}}(L) = \frac{\eta}{2} r(i) \langle \mathbf{r}^{\text{val}}, \boldsymbol{\Psi}_{\text{val}}^\text{T} \mathbf{P}_\Psi \boldsymbol{\psi}(\mathbf{x}_i) \rangle. \quad (19)$$

486 REFERENCES  
487

488 Mingyao Ai, Jun Yu, Huiming Zhang, and HaiYing Wang. Optimal subsampling algorithms for big  
489 data regressions. *Statistica Sinica*, 31(2):749–772, 2021.

490 AI@Meta. Llama 3 model card. 2024. URL [https://github.com/meta-llama/llama3/blob/main/MODEL\\_CARD.md](https://github.com/meta-llama/llama3/blob/main/MODEL_CARD.md).

491 Kyriakos Axiotis, Vincent Cohen-Addad, Monika Henzinger, Sammy Jerome, Vahab Mirrokni,  
492 David Saulpic, David Woodruff, and Michael Wunder. Data-efficient learning via clustering-  
493 based sensitivity sampling: Foundation models and beyond. *arXiv preprint arXiv:2402.17327*,  
494 2024.

495 Juhan Bae, Wu Lin, Jonathan Lorraine, and Roger Grosse. Training data attribution via approximate  
496 unrolled differentiation. *arXiv:2405.12186*, 2024.

497 Peter L Bartlett, Andrea Montanari, and Alexander Rakhlin. Deep learning: a statistical viewpoint.  
498 *Acta numerica*, 30:87–201, 2021.

499 Hyung Won Chung, Le Hou, Shayne Longpre, Barret Zoph, Yi Tay, William Fedus, Yunxuan Li,  
500 Xuezhi Wang, Mostafa Dehghani, Siddhartha Brahma, et al. Scaling instruction-finetuned lan-  
501 guage models. *Journal of Machine Learning Research*, 25(70):1–53, 2024.

502 Alexis Conneau, Kartikay Khandelwal, Naman Goyal, Vishrav Chaudhary, Guillaume Wenzek,  
503 Francisco Guzmán, Edouard Grave, Myle Ott, Luke Zettlemoyer, and Veselin Stoyanov. Un-  
504 supervised cross-lingual representation learning at scale. *CoRR*, abs/1911.02116, 2019. URL  
505 <http://arxiv.org/abs/1911.02116>.

506 Logan Engstrom, Axel Feldmann, and Aleksander Madry. Dsdm: Model-aware dataset selection  
507 with datamodels. *arXiv preprint arXiv:2401.12926*, 2024.

508 Logan Engstrom, Andrew Ilyas, Benjamin Chen, Axel Feldmann, William Moses, and Aleksander  
509 Madry. Optimizing ml training with metagradient descent. *arXiv preprint arXiv:2503.13751*,  
510 2025.

511 Alex Fang, Albin Madappally Jose, Amit Jain, Ludwig Schmidt, Alexander Toshev, and Vaishaal  
512 Shankar. Data filtering networks. *arXiv preprint arXiv:2309.17425*, 2023.

513 Suchin Gururangan, Ana Marasović, Swabha Swayamdipta, Kyle Lo, Iz Beltagy, Doug Downey,  
514 and Noah A Smith. Don’t stop pretraining: Adapt language models to domains and tasks. *arXiv  
515 preprint arXiv:2004.10964*, 2020.

516 Edward J Hu, Phillip Wallis, Zeyuan Allen-Zhu, Yuanzhi Li, Shean Wang, Lu Wang, Weizhu Chen,  
517 et al. Lora: Low-rank adaptation of large language models. In *International Conference on  
518 Learning Representations*, 2022.

519 Andrew Ilyas, Sung Min Park, Logan Engstrom, Guillaume Leclerc, and Aleksander Madry. Data-  
520 models: Predicting predictions from training data. In *Proceedings of the 39th International Con-  
521 ference on Machine Learning*, 2022.

522 Germain Kolossov, Andrea Montanari, and Pulkit Tandon. Towards a statistical theory of data  
523 selection under weak supervision. In *The Twelfth International Conference on Learning Repre-  
524 sentations*, 2024.

525 Wing Lian, Guan Wang, Bleys Goodson, Eugene Pentland, Austin Cook, Chanvichet Vong, and  
526 “Teknium”. Slimorca: An open dataset of gpt-4 augmented flan reasoning traces, with verifica-  
527 tion, 2023. URL <https://huggingface.co/Open-Orca/SlimOrca>.

528 Zifan Liu, Amin Karbasi, and Theodoros Rekatsinas. Tsds: Data selection for task-specific model  
529 finetuning. *Advances in Neural Information Processing Systems*, 37:10117–10147, 2024.

530 Shayne Longpre, Le Hou, Tu Vu, Albert Webson, Hyung Won Chung, Yi Tay, Denny Zhou, Quoc V  
531 Le, Barret Zoph, Jason Wei, et al. The flan collection: Designing data and methods for effective  
532 instruction tuning. In *International Conference on Machine Learning*, pp. 22631–22648. PMLR,  
533 2023.

540 Subhabrata Mukherjee, Arindam Mitra, Ganesh Jawahar, Sahaj Agarwal, Hamid Palangi, and  
 541 Ahmed Awadallah. Orca: Progressive learning from complex explanation traces of gpt-4, 2023.  
 542

543 Long Ouyang, Jeffrey Wu, Xu Jiang, Diogo Almeida, Carroll Wainwright, Pamela Mishkin, Chong  
 544 Zhang, Sandhini Agarwal, Katarina Slama, Alex Ray, et al. Training language models to fol-  
 545 low instructions with human feedback. *Advances in neural information processing systems*, 35:  
 546 27730–27744, 2022.

547 Sung Min Park, Kristian Georgiev, Andrew Ilyas, Guillaume Leclerc, and Aleksander Madry. Trak:  
 548 Attributing model behavior at scale. *arXiv preprint arXiv:2303.14186*, 2023.

549 Baolin Peng, Chunyuan Li, Pengcheng He, Michel Galley, and Jianfeng Gao. Instruction tuning  
 550 with gpt-4. *arXiv preprint arXiv:2304.03277*, 2023.

551 Garima Pruthi, Frederick Liu, Satyen Kale, and Mukund Sundararajan. Estimating training data  
 552 influence by tracing gradient descent. *Advances in Neural Information Processing Systems*, 33:  
 553 19920–19930, 2020.

554 Noveen Sachdeva, Benjamin Coleman, Wang-Cheng Kang, Jianmo Ni, Lichan Hong, Ed H Chi,  
 555 James Caverlee, Julian McAuley, and Derek Zhiyuan Cheng. How to train data-efficient llms.  
 556 *arXiv preprint arXiv:2402.09668*, 2024.

557 Andrea Schioppa, Katja Filippova, Ivan Titov, and Polina Zablotskaia. Theoretical and practical  
 558 perspectives on what influence functions do. *Advances in Neural Information Processing Systems*,  
 559 36:27560–27581, 2023.

560 Rohan Taori, Ishaan Gulrajani, Tianyi Zhang, Yann Dubois, Xuechen Li, Carlos Guestrin, Percy  
 561 Liang, and Tatsunori B. Hashimoto. Stanford alpaca: An instruction-following llama model.  
 562 [https://github.com/tatsu-lab/stanford\\_alpaca](https://github.com/tatsu-lab/stanford_alpaca), 2023.

563 Simone Tedeschi and Roberto Navigli. MultiNERD: A multilingual, multi-genre and fine-grained  
 564 dataset for named entity recognition (and disambiguation). In *Findings of the Association  
 565 for Computational Linguistics: NAACL 2022*, pp. 801–812, Seattle, United States, July 2022.  
 566 Association for Computational Linguistics. doi: 10.18653/v1/2022.findings-naacl.60. URL  
 567 <https://aclanthology.org/2022.findings-naacl.60>.

568 Daniel Ting and Eric Brochu. Optimal subsampling with influence functions. *Advances in neural  
 569 information processing systems*, 31, 2018.

570 Aaad W van der Vaart. *Asymptotic Statistics*. Cambridge University Press, 2000.

571 HaiYing Wang, Rong Zhu, and Ping Ma. Optimal subsampling for large sample logistic regression.  
 572 *Journal of the American Statistical Association*, 113(522):829–844, 2018.

573 Yizhong Wang, Hamish Ivison, Pradeep Dasigi, Jack Hessel, Tushar Khot, Khyathi Chandu, David  
 574 Wadden, Kelsey MacMillan, Noah A Smith, Iz Beltagy, et al. How far can camels go? exploring  
 575 the state of instruction tuning on open resources. *Advances in Neural Information Processing  
 576 Systems*, 36:74764–74786, 2023.

577 Zifeng Wang, Hong Zhu, Zhenhua Dong, Xiuqiang He, and Shao-Lun Huang. Less is better: Un-  
 578 weighted data subsampling via influence function. In *Proceedings of the AAAI Conference on  
 579 Artificial Intelligence*, volume 34, pp. 6340–6347, 2020.

580 Mengzhou Xia, Sadhika Malladi, Suchin Gururangan, Sanjeev Arora, and Danqi Chen. LESS:  
 581 selecting influential data for targeted instruction tuning. In *Proceedings of the 41st International  
 582 Conference on Machine Learning*, pp. 54104–54132, 2024.

583 Sang Michael Xie, Shibani Santurkar, Tengyu Ma, and Percy S Liang. Data selection for language  
 584 models via importance resampling. *Advances in Neural Information Processing Systems*, 36:  
 585 34201–34227, 2023.

586 Chunting Zhou, Pengfei Liu, Puxin Xu, Srinivasan Iyer, Jiao Sun, Yuning Mao, Xuezhe Ma, Avia  
 587 Efrat, Ping Yu, Lili Yu, et al. Lima: Less is more for alignment. *Advances in Neural Information  
 588 Processing Systems*, 36, 2024.

594 **A ADDITIONAL EXPERIMENTAL DETAILS AND RESULTS**  
 595

596 **A.1 EXPERIMENTS FOR TOKEN-BASED LEARNING**  
 597

598 In these experiments, we used pretrained models as base models and constructed training, validation,  
 599 and test sets from real-world datasets. Details of the datasets and models are provided in Section J.  
 600

601 For each training example count—both for surrogate model training (used for scoring) and final  
 602 model training—we selected the learning rate from the following grid:  
 603

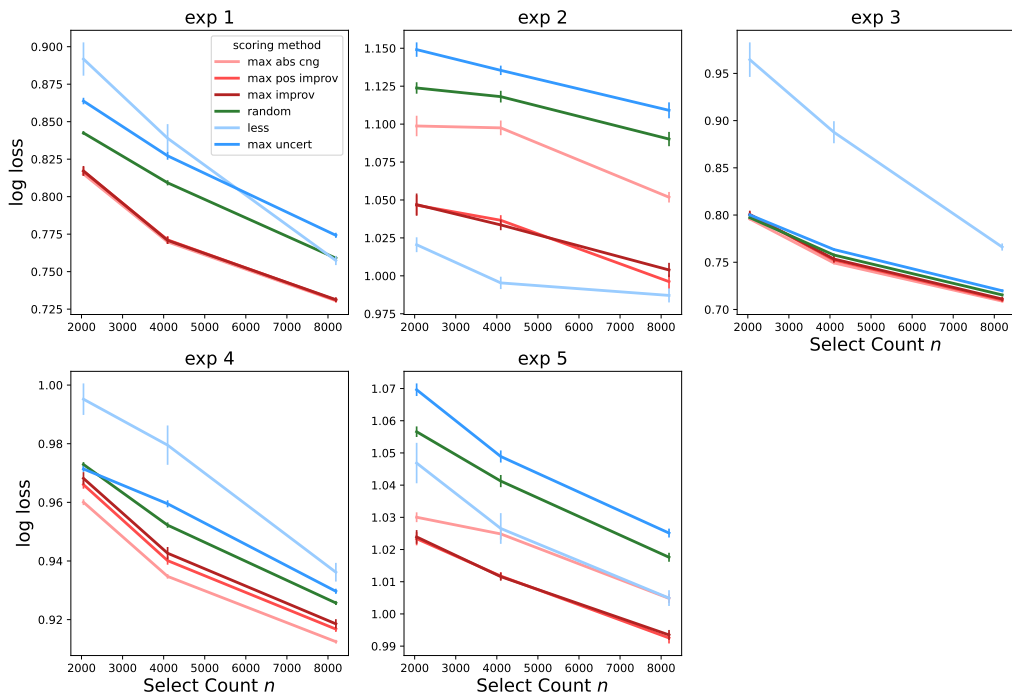
$$[3e-6, 1e-5, 3e-5, 1e-4, 3e-4, 1e-3, 3e-3, 1e-2].$$

604 The optimal learning rate was determined by training models on randomly sampled subsets from the  
 605 training pool and evaluating their test log-loss. For each learning rate, the loss was averaged over 10  
 606 runs, with a new random subset used in each run. The best-performing learning rate was selected  
 607 separately for each experimental configuration listed in Table 1 and Table 2.  
 608

609 **Implementation details for Less (Xia et al., 2024)** We used the public implementation from the  
 610 authors’ GitHub repository. The projection dimension was set to 8192. Learning rate and other  
 611 hyperparameters were tuned identically for all approaches. For both our method and LESS, the  
 612 surrogate model used the same number of samples and was trained for four epochs, matching the  
 613 settings in the LESS paper. Following the original LESS procedure, we selected the top-scoring  
 614 examples.  
 615

616 **A.2 EXPANDED RESULTS FOR INSTRUCTION TUNING**  
 617

618 In the main paper, we compared our scoring methods for the SCORE+RANDOM strategy. Due to  
 619 space constraints, Figure 2 omitted results for Experiment 3. In Figure 4, we provide an expanded  
 620 version that includes results for Experiment 3 as well.  
 621  
 622



647 Figure 4: Expanded version of Figure 2 including the Experiment 3 plot.  
 648

648  
649

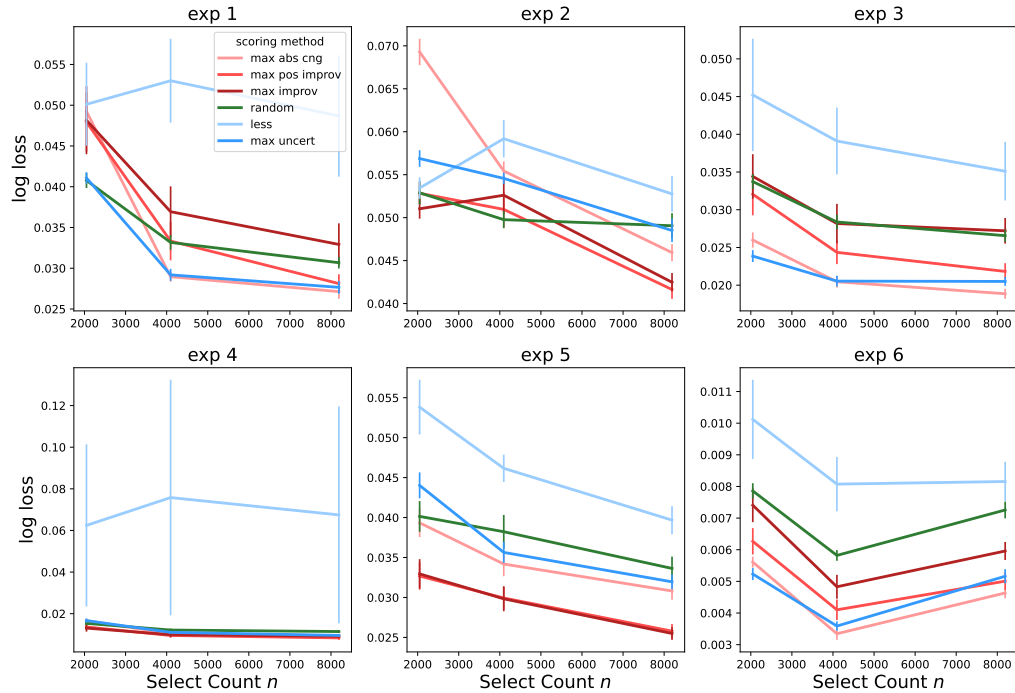
## A.3 EXPANDED RESULTS FOR NAMED ENTITY RECOGNITION

650  
651

In Figure 3 of the main paper, we reported results for SCORE+RANDOM using a fixed selected sample size of  $n = 8 \times 1024$ , across all experiment configurations in Table 2.

652  
653  
654

In Figure 5, we show how the test log-loss varies with the selected sample size  $n$  for different scoring methods under the SCORE+RANDOM strategy, and how these compare to random selection.

655  
656

657

Figure 5: Test log-loss vs. number of selected samples  $n$  for NER. Lines show mean log-loss over 10 runs; error bars are  $\pm 1$  standard error. Results use Method A with the SCORE+RANDOM strategy.

660

661

## B COMPARISON OF SCORE+RANDOM AND SCORE-ONLY SELECTION

662

663

In this section we examine how the performance of our strategies changes when all training examples are selected from the top-scoring set (SCORE-ONLY) instead of selecting only half of them from the top and the other half at random (SCORE+RANDOM).

664

Recall that our scores approximate how much benefit each example provides when added to a randomly chosen pool of training data. A higher score therefore indicates an example expected to be more helpful in that setting. SCORE+RANDOM selects half of the final training set from the highest-scoring examples and fills the rest with random examples, whereas SCORE-ONLY takes only the top-scoring examples. This design creates a trade-off:

665

666

667

668

669

670

671

672

673

674

675

676

677

- Pure exploitation: Selecting only top-scoring examples can maximize immediate gain because every chosen example has a high estimated contribution.
- Score validity and diversity: The scores are defined relative to adding examples to a random pool. If we select only top examples, the resulting set may differ substantially from the random reference, making the scores a less accurate guide. Randomly adding half the examples keeps the final set closer to the conditions under which the scores were computed and also protects against loss of diversity.

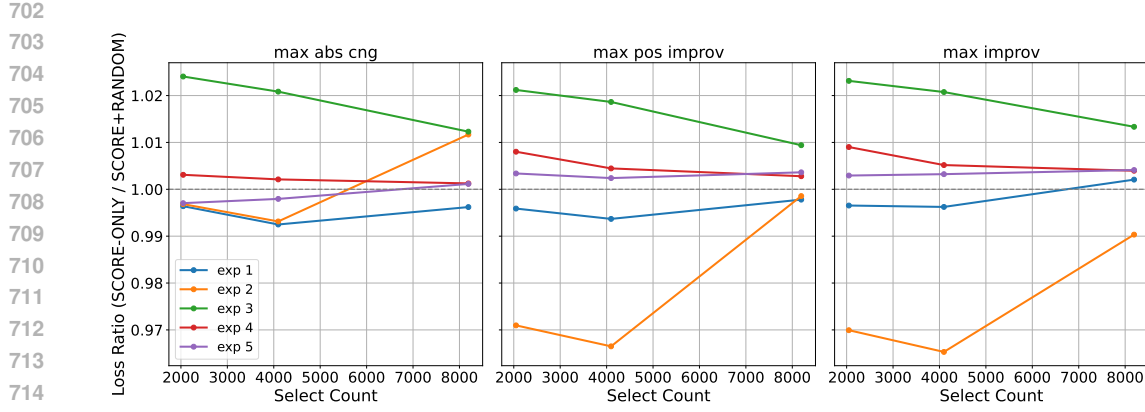


Figure 6: Ratio of log loss for SCORE-ONLY versus SCORE+RANDOM across our three scoring strategies and all instruction-tuning setups in Table 1. Scores are computed using Algorithm 1.

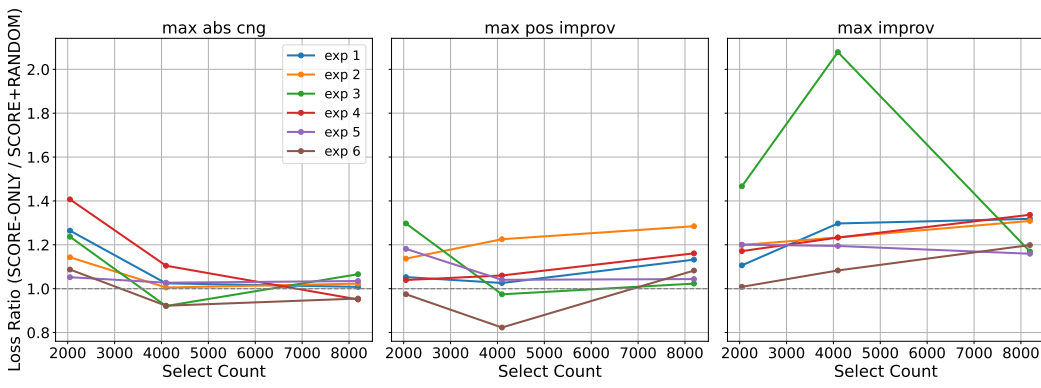


Figure 7: Ratio of log-loss for SCORE-ONLY versus SCORE+RANDOM across our three scoring strategies and all NER setups in Table 2. Scores are computed using Algorithm 1.

Which effect dominates varies by task.

Figures 6 and 7 show the ratio of log-loss for the two selection strategies in instruction tuning and NER respectively. In each figure the three subplots correspond to our three scoring strategies; different lines indicate the various experimental setups. Algorithm 1 is used to obtain the scores.

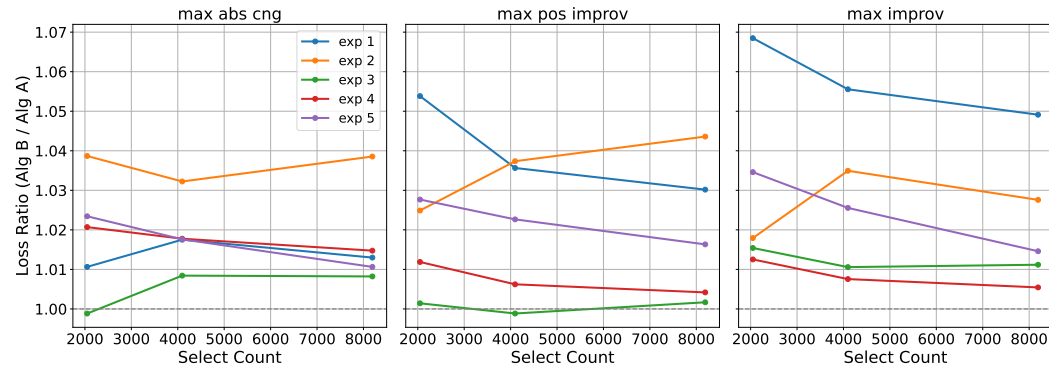
For instruction tuning, SCORE+RANDOM performs better in three setups (3, 4, 5), while SCORE-ONLY is better in the remaining two (1, 2) across most selection sizes and scoring methods. For NER, SCORE+RANDOM tends to outperform SCORE-ONLY more often, particularly for the Max-Improvement scores.

## C METHOD B VS METHOD A

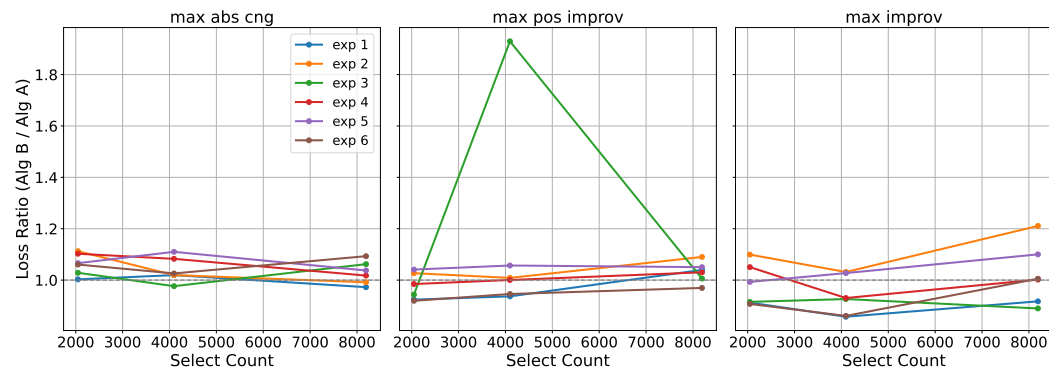
All previous plots used Method A (Algorithm 1) for scoring. Here we compare the performance of the two scoring methods: Method A (Algorithm 1) and Method B (Algorithm 2)—across our experiments, using the SCORE+RANDOM selection strategy for both.

Figures 8 and 9 show the ratio of test log-loss obtained with Method B relative to Method A for instruction tuning and NER, respectively. Each figure contains three subplots corresponding to our three scoring strategies, and different lines represent the various experimental setups.

756 The results indicate that for instruction tuning, Method A is most often superior, while for NER  
 757 there is no consistent winner. A possible explanation is that Method B uses two distinct training  
 758 trajectories. Our analysis assumes that the resulting models differ only slightly, but in practice, the  
 759 two training trajectories can diverge substantially. This effect is likely to be stronger with large and  
 760 highly overparameterized models such as Meta-Llama-3-8B, which we used for instruction tuning.  
 761 We expect the larger distance between the two models to result in less accurate score estimation in  
 762 Method B, as compared to Method A.



778 Figure 8: Ratio of test log-loss using Method B (Algorithm 2) to Method A (Algorithm 1) for  
 779 instruction tuning. Results use the SCORE+RANDOM selection strategy. Each subplot corresponds  
 780 to one scoring strategy; lines denote different experimental setups in Table 1.



796 Figure 9: Ratio of test log-loss using Method B (Algorithm 2) to Method A (Algorithm 1) for  
 797 NER. Results use the SCORE+RANDOM selection strategy. Each subplot corresponds to one scoring  
 798 strategy; lines denote different experimental setups in Table 2.

## D LOGISTIC REGRESSION EXPERIMENTS

803 In these experiments, we synthetically generated the training pool, validation set, and test set. We  
 804 begin by defining a parametric family of distributions used to construct the data.

805 For a given  $p > 0$  and parameter vector  $\theta \in \mathbb{R}^p$ , we define a distribution  $\mathcal{P}_\theta$  over pairs  $(x, y)$ , where  
 806  $x \in \mathbb{R}^p$  and  $y \in \{0, 1\}$ . The features are sampled as  $x \sim \mathcal{N}(0, I)$ , and the label  $y$  is drawn according  
 807 to a logistic model:

$$809 \Pr(y = 1 \mid x) = \frac{1}{1 + \exp(-x \cdot \theta)}, \quad \Pr(y = 0 \mid x) = 1 - \Pr(y = 1 \mid x).$$

We randomly sample a unit vector  $\theta^*$  from the unit sphere to serve as the target direction. A second unit vector  $\theta'$  is then drawn such that it lies at an angle  $\gamma$  from  $\theta^*$ . In our experiments, we set  $p = 10$  and  $\gamma = \pi/2$ .

The training pool consists of  $N = 128 \times 1024$  samples, drawn independently from the mixture distribution:

$$\mathcal{D}_{\text{train}} = \frac{1}{2}\mathcal{P}_{\theta^*} + \frac{1}{2}\mathcal{P}_{\theta'}.$$

The validation and test sets contain  $m_{\text{val}} = 1024$  and  $m_{\text{test}} = 10,000$  samples respectively, both drawn i.i.d. from the target distribution  $\mathcal{P}_{\theta^*}$ .

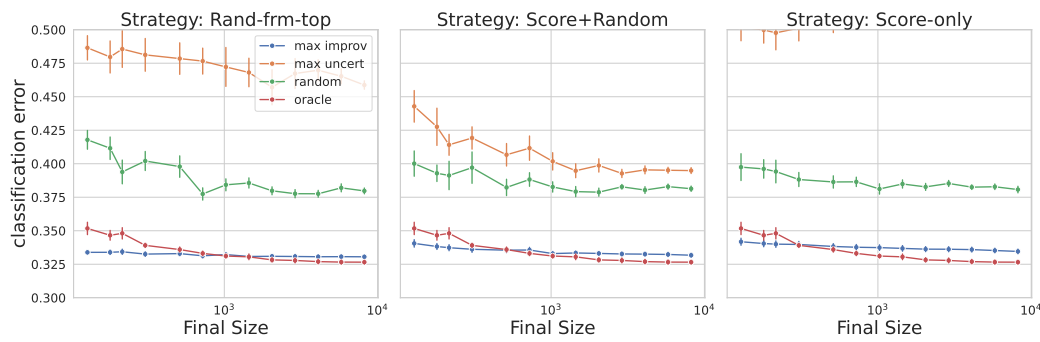


Figure 10: Data selection experiments with Method B for logistic regression on synthetic data in  $d = 10$  dimensions (4 epochs of training). Each color corresponds to a distinct method to score data in the training pool, and each frame to a distinct method to use the score to form the selected set. Each symbol corresponds to the average of 10 experiments.

For scoring, we used Method B as described in Algorithm 2; similar experiments with Method A produced comparable results, so we report only Method B here. Algorithm 2 does not specify the method to select data on the basis of scores. In Figure 10 we compare SCORE-ONLY and SCORE+RANDOM (already introduced above) with a third one RANDOM-FROM-TOP that selects at random from the top 50% subset of data with highest scores.

The RANDOM-FROM-TOP method is included only for these synthetic logistic-regression experiments, for theoretical interest as by construction, the training pool contains half of its examples from the target distribution.

The base set used for initial training contains  $|U| = 4 \times 1024$  examples.

For both the scoring model and the final model training, we used 4 epochs of batch gradient descent with a linear decay learning rate scheduler. The initial learning rate was set to 0.5. We used  $\epsilon = \frac{1}{10}$  for adjusting the learning rate on validation examples.

The selected subset size  $n$  was varied from 128 to 8192 in multiplicative steps of  $\sqrt{2}$ . All results are averaged over 10 independent runs. The final performance curves are presented in Figure 10.

## E PROOF OF PROPOSITION 1

Throughout this proof, we denote by  $C$  a generic constant that can depend on  $c_0, C_1, M, C_\eta$  and whose value is allowed to change from line to line.

Letting  $\Delta_s(i) = \hat{\theta}_s^{\text{bas}+i} - \hat{\theta}_s^{\text{bas}}$ , Eq. (11) yields

$$\begin{aligned} \Delta_{k+1}(i) &= \Delta_k(i) - \eta m \nabla^2 \hat{R}_U(\hat{\theta}_k^{\text{bas}}) \Delta_k(i) - \eta \nabla \ell(\hat{\theta}_k^{\text{bas}}; \mathbf{x}_i) + \text{err}_k(i) \\ &= \mathbf{H}_k \Delta_k(i) - \eta \nabla \ell(\hat{\theta}_k^{\text{bas}}; \mathbf{x}_i) + \text{err}_k(i), \end{aligned} \quad (20)$$

864 where  $\mathbf{H}_k$  is defined as in Eq. (14) and  
 865

$$866 \text{err}_k(i) := -\eta [\nabla \ell(\hat{\boldsymbol{\theta}}_k^{\text{bas}+i}; \mathbf{x}_i) - \nabla \ell(\hat{\boldsymbol{\theta}}_k^{\text{bas}}; \mathbf{x}_i)] - \eta m \int_0^1 [\nabla^2 \hat{R}_U(\bar{\boldsymbol{\theta}}_k(z)) - \nabla^2 \hat{R}_U(\hat{\boldsymbol{\theta}}_k^{\text{bas}})] \Delta_k(i) dz,$$

868 where  $\bar{\boldsymbol{\theta}}_k(z) = (1-z)\hat{\boldsymbol{\theta}}_k^{\text{bas}} + z\hat{\boldsymbol{\theta}}_k^{\text{bas}+i}$ . By assumption  $\boldsymbol{\theta} \mapsto \nabla \ell(\boldsymbol{\theta}; \mathbf{x}_i)$  and  $\boldsymbol{\theta} \mapsto \nabla^2 \hat{R}_U(\boldsymbol{\theta})$  are  
 869  $M$ -Lipschitz, whence  
 870

$$871 \|\text{err}_k(i)\| \leq \eta M \|\hat{\boldsymbol{\theta}}_k^{\text{bas}+i} - \hat{\boldsymbol{\theta}}_k^{\text{bas}}\| + \eta m M \|\hat{\boldsymbol{\theta}}_k^{\text{bas}+i} - \hat{\boldsymbol{\theta}}_k^{\text{bas}}\| \|\Delta_k(i)\| \\ 872 = \eta M \|\Delta_k(i)\| + \eta m M \|\Delta_k(i)\|^2. \quad (21)$$

874 Define  $\Delta_k^{\text{lin}}(i)$  by letting  $\Delta_k^{\text{lin}}(i) = \mathbf{0}$  and, for  $k \geq 0$ ,  
 875

$$876 \Delta_{k+1}^{\text{lin}}(i) = \mathbf{H}_k \Delta_k^{\text{lin}}(i) - \eta \nabla \ell(\hat{\boldsymbol{\theta}}_k^{\text{bas}}; \mathbf{x}_i). \quad (22)$$

877 Comparing with Eq. (20), we obtain  
 878

$$879 (\Delta_{k+1}(i) - \Delta_{k+1}^{\text{lin}}(i)) = \mathbf{H}_k (\Delta_{k+1}(i) - \Delta_{k+1}^{\text{lin}}(i)) + \text{err}_k(\eta, m), \\ 880 \Rightarrow \Delta_t(i) - \Delta_t^{\text{lin}}(i) = \sum_{s=0}^{t-1} \mathbf{M}_{t,s+1} \text{err}_s(\eta, m). \quad (23)$$

883 Since  $\nabla^2 \hat{R}_U(\hat{\boldsymbol{\theta}}_k^{\text{bas}}) \succeq c_0 \mathbf{I}_d$ , we have  $\|\mathbf{H}_k\|_{\text{op}} \leq (1 - c_0 m \eta)$ , and therefore  
 884

$$885 \|\Delta_t(i) - \Delta_t^{\text{lin}}(i)\| \leq \sum_{s=0}^{t-1} \|\mathbf{M}_{t,s+1}\|_{\text{op}} \|\text{err}_s(\eta, m)\| \\ 886 \leq \sum_{s=0}^{t-1} (1 - c_0 m \eta)^{t-s-1} \|\text{err}_s(\eta, m)\|. \quad (24)$$

889 Further, from Eq. (22), and using  $\|\nabla \ell(\hat{\boldsymbol{\theta}}_k^{\text{bas}}; \mathbf{x}_i)\| \leq C_1$ , we get  
 890

$$891 \Delta_t^{\text{lin}}(i) = -\eta \sum_{s=0}^{t-1} \mathbf{M}_{t,s+1} \nabla \ell(\hat{\boldsymbol{\theta}}_s^{\text{bas}}; \mathbf{x}_i), \\ 892 \Rightarrow \|\Delta_t^{\text{lin}}(i)\| \leq C_1 \eta \sum_{s=0}^{t-1} (1 - c_0 m \eta)^{t-s-1} \leq \frac{C}{m}. \quad (25)$$

900 Let  $D_t(i) := \max_{s \leq t} \|\Delta_s(i)\|$ ,  $E_t(i) := \max_{s \leq t} \|\text{err}_s(i)\|$ . Using Eqs. (21), (24) and (25), we get  
 901

$$902 D_t(i) \leq \frac{C}{m} + \frac{1}{c_0 m \eta} E_{t-1}(i), \\ 903 E_t(i) \leq \eta M D_t(i) + \eta m M D_t(i)^2.$$

905 Using these inequalities together, we obtain, for all  $m \geq m_0$  (and eventually adjusting the constant  
 906  $C$ )  
 907

$$908 D_t(i) \leq \frac{C}{m}, \quad E_t(i) \leq \frac{C \eta}{m}, \quad (26)$$

910 whence, using again Eq. (24), we get  
 911

$$912 \|\Delta_t(i) - \Delta_t^{\text{lin}}(i)\| \leq \frac{C}{m^2}. \quad (27)$$

914 Notice that we can rewrite  
 915

$$916 S_i^{\text{lin}} = -\frac{1}{L} \sum_{s=1}^L \langle \nabla \hat{R}_{\text{val}}(\hat{\boldsymbol{\theta}}_s^{\text{bas}}), \Delta_s^{\text{lin}}(i) \rangle, \quad (28)$$

whence, using the fact that  $\|\nabla^2 \widehat{R}_{\text{val}}(\bar{\boldsymbol{\theta}})\|_{\text{op}} \leq C$  for all  $\bar{\boldsymbol{\theta}} \in [\hat{\boldsymbol{\theta}}_k^{\text{bas}}, \hat{\boldsymbol{\theta}}_k^{\text{bas}+i}]$  (this follows from the assumed bound  $\|\nabla^2 \widehat{R}_{\text{val}}(\hat{\boldsymbol{\theta}}_k^{\text{bas}})\|_{\text{op}} \leq C_1$  and the Lipschitz property of  $\boldsymbol{\theta} \mapsto \nabla^2 \widehat{R}_{\text{val}}(\hat{\boldsymbol{\theta}})$ ), we get

$$\begin{aligned} |S_i - S_i^{\text{lin}}| &\leq C \max_{s \leq L} \|\Delta_s(i)\|^2 + \frac{1}{L} \sum_{s=1}^L |\langle \nabla \widehat{R}_{\text{val}}(\hat{\boldsymbol{\theta}}_s^{\text{bas}}), \Delta_s(i) - \Delta_s^{\text{lin}}(i) \rangle| \\ &\leq C \max_{s \leq L} \|\Delta_s(i)\|^2 + C \max_{s \leq L} \|\Delta_s(i) - \Delta_s^{\text{lin}}(i)\| \\ &\leq \frac{C}{m^2}, \end{aligned}$$

and this completes the proof.

## F PROOF OF THEOREM 1

Throughout this proof, we denote by  $C$  a generic constant that can depend on  $c_0, C_1, M, C_\eta$  and whose value is allowed to change from line to line.

### F.1 BOUND ON $\Upsilon_i$

The iteration for  $\hat{\boldsymbol{\theta}}_k^{\text{bas}}$  and  $\hat{\boldsymbol{\theta}}_k^{\text{bas},+}$ , as specified by Algorithm 2, reads

$$\hat{\boldsymbol{\theta}}_{k+1}^{\text{bas}} = \hat{\boldsymbol{\theta}}_k^{\text{bas}} - \eta m \nabla \widehat{R}_U(\hat{\boldsymbol{\theta}}_k^{\text{bas}}), \quad (29)$$

$$\hat{\boldsymbol{\theta}}_{k+1}^{\text{bas},+} = \hat{\boldsymbol{\theta}}_{0,k+1}^{\text{bas},+} - \varepsilon \eta m_{\text{val}} \nabla \widehat{R}_{\text{val}}(\hat{\boldsymbol{\theta}}_{0,k+1}^{\text{bas},+}), \quad \hat{\boldsymbol{\theta}}_{0,k+1}^{\text{bas},+} = \hat{\boldsymbol{\theta}}_k^{\text{bas},+} - \eta m \nabla \widehat{R}_U(\hat{\boldsymbol{\theta}}_k^{\text{bas},+}). \quad (30)$$

Letting  $\Delta_k := \hat{\boldsymbol{\theta}}_k^{\text{bas},+} - \hat{\boldsymbol{\theta}}_k^{\text{bas}}$ , and  $\Delta_{0,k} := \hat{\boldsymbol{\theta}}_{0,k}^{\text{bas},+} - \hat{\boldsymbol{\theta}}_k^{\text{bas}}$ , we obtain

$$\Delta_{k+1} = \Delta_{0,k+1} - \varepsilon \eta m_{\text{val}} \nabla \widehat{R}_{\text{val}}(\hat{\boldsymbol{\theta}}_{k+1}^{\text{bas}}) + \text{err}_{k+1}^{(1)}, \quad (31)$$

$$\Delta_{0,k+1} = \mathbf{H}_k \Delta_k + \text{err}_k^{(2)}. \quad (32)$$

where, letting  $\bar{\boldsymbol{\theta}}_{0,k+1}(z) = (1-z)\hat{\boldsymbol{\theta}}_{k+1}^{\text{bas}} + z\hat{\boldsymbol{\theta}}_{0,k+1}^{\text{bas},+}$  and  $\bar{\boldsymbol{\theta}}_k(z) = (1-z)\hat{\boldsymbol{\theta}}_k^{\text{bas}} + z\hat{\boldsymbol{\theta}}_k^{\text{bas},+}$ , we have

$$\text{err}_{k+1}^{(1)} := -\eta \varepsilon m_{\text{val}} \int_0^1 \nabla^2 \widehat{R}_{\text{val}}(\bar{\boldsymbol{\theta}}_{0,k+1}(z)) \Delta_{0,k+1} dz,$$

$$\text{err}_k^{(2)} := -\eta m \int_0^1 [\nabla^2 \widehat{R}_U(\bar{\boldsymbol{\theta}}_k(z)) - \nabla^2 \widehat{R}_U(\hat{\boldsymbol{\theta}}_k^{\text{bas}})] \Delta_k dz.$$

Using the assumption that  $\|\nabla^2 \widehat{R}_{\text{val}}(\hat{\boldsymbol{\theta}}_{k+1}^{\text{bas}}(z))\|_{\text{op}} \leq C$  and  $\boldsymbol{\theta} \mapsto \nabla^2 \widehat{R}_{\text{val}}(\boldsymbol{\theta})$  is  $M$ -Lipschitz, we get:

$$\|\text{err}_{k+1}^{(1)}\| \leq C \varepsilon \eta m_{\text{val}} \{ \|\Delta_{0,k+1}\| + \|\Delta_{0,k+1}\|^2 \}. \quad (33)$$

On the other hand, since  $\boldsymbol{\theta} \mapsto \nabla^2 \widehat{R}_U(\boldsymbol{\theta})$  is also  $M$ -Lipschitz, we have

$$\|\text{err}_k^{(2)}\| \leq \eta m M \|\Delta_k\|^2, \quad (34)$$

whence, using Eq. (32) and  $\|\mathbf{H}_k\|_{\text{op}} \leq 1$

$$\begin{aligned} \|\Delta_{0,k+1}\| &\leq \|\Delta_k\| + \eta m M \|\Delta_k\|^2 \\ \Rightarrow \|\text{err}_{k+1}^{(1)}\| &\leq C \varepsilon \eta m_{\text{val}} \{ \|\Delta_k\| + \|\Delta_k\|^2 + \eta^2 m^2 \|\Delta_k\|^4 \}, \end{aligned} \quad (35)$$

where in the last line we used the assumption that  $\eta m \leq C_\eta$ .

Substituting Eqs. (34) and (35) in Eq. (31), (32), we obtain (using again  $\eta m \leq C_\eta$ )

$$\Delta_{k+1} = \mathbf{H}_k \Delta_k - \varepsilon \eta m_{\text{val}} \nabla \widehat{R}_{\text{val}}(\hat{\boldsymbol{\theta}}_{k+1}^{\text{bas}}) + \text{err}_k, \quad (36)$$

$$\|\text{err}_k\| \leq C \eta \varepsilon m_{\text{val}} (\|\Delta_k\| + \|\Delta_k\|^4) + C \eta m \|\Delta_k\|^2. \quad (37)$$

We define  $\Delta_k^{\text{lin}} = \mathbf{0}$  and, for  $k \geq 0$ ,

$$\Delta_{k+1}^{\text{lin}} = \mathbf{H}_k \Delta_k^{\text{lin}} - \varepsilon \eta m_{\text{val}} \nabla \widehat{R}_{\text{val}}(\hat{\boldsymbol{\theta}}_{k+1}^{\text{bas}}), \quad (38)$$

972 whence

973

$$\Delta_t^{\text{lin}} = -\varepsilon\eta m_{\text{val}} \sum_{s=0}^{t-1} M_{t,s+1} \nabla \hat{R}_{\text{val}}(\hat{\theta}_{s+1}^{\text{bas}}), \quad \Delta_t - \Delta_t^{\text{lin}} = \sum_{s=0}^{t-1} M_{t,s+1} \text{err}_s. \quad (39)$$

974

975 Define  $D_t := \max_{s \leq t} \|\Delta_s\|$ ,  $E_t := \max_{s \leq t} \|\text{err}_s\|$ . Using the fact that  $\|M_{t,s+1}\|_{\text{op}} \leq (1 - c_0 m \eta)^{t-s-1}$  and the assumption  $\|\nabla \hat{R}_{\text{val}}(\hat{\theta}_k^{\text{bas}})\| \leq C_1$ , we get, from Eqs. (37), (39),

976

977

$$D_{t+1} \leq \frac{C\varepsilon m_{\text{val}}}{m} + \frac{C}{m\eta} E_t, \quad (40)$$

978

979

$$E_t \leq C\eta\varepsilon m_{\text{val}}(D_t + D_t^4) + C\eta m D_t^2, \quad (41)$$

980

981 Using the assumption  $\varepsilon m_{\text{val}}/m \leq c_*$ , this is easily seen to imply

982

983

$$D_t \leq C \frac{\varepsilon m_{\text{val}}}{m}, \quad E_t \leq C \frac{(\varepsilon m_{\text{val}})^2}{m} \eta. \quad (42)$$

984

985 Substituting in Eq. (39), we get

986

987

$$\|\Delta_t - \Delta_t^{\text{lin}}\| \leq \sum_{s=0}^{t-1} (1 - c_0 m \eta)^{t-s-1} \|\text{err}_s\| \leq C \left( \frac{\varepsilon m_{\text{val}}}{m} \right)^2. \quad (43)$$

988

989 The linearized score of Eq. (16) can be rewritten as

990

991

$$\Upsilon_i^{\text{lin}} \varepsilon = -\frac{1}{L} \sum_{s=1}^L \langle \nabla \ell(\hat{\theta}_s^{\text{bas}}; \mathbf{x}_i), \Delta_s^{\text{lin}} \rangle. \quad (44)$$

992

993 Using the fact that  $\|\nabla \ell(\hat{\theta}_k^{\text{bas}}, \mathbf{x}_i)\|, \|\nabla \ell(\hat{\theta}_k^{\text{bas}}, \mathbf{x}_i)\|_{\text{op}} \leq C_1$ , we get

994

995

$$|\Upsilon_i(\varepsilon) - \Upsilon_i^{\text{lin}} \varepsilon| \leq \frac{1}{L} \sum_{s=1}^L \left| \ell(\hat{\theta}_k^{\text{bas}}; \mathbf{x}_i) - \ell(\hat{\theta}_k^{\text{bas},+}; \mathbf{x}_i) + \langle \nabla \ell(\hat{\theta}_s^{\text{bas}}; \mathbf{x}_i), \Delta_s^{\text{lin}} \rangle \right| \quad (45)$$

996

997

$$\leq \frac{C}{L} \sum_{s=1}^L \|\Delta_s\|^2 + \frac{C}{L} \sum_{s=1}^L \|\Delta_s - \Delta_s^{\text{lin}}\| \quad (46)$$

998

999

$$\leq C \left( \frac{\varepsilon m_{\text{val}}}{m} \right)^2, \quad (47)$$

1000

## F.2 BOUND ON $\phi_i$

1001 The iteration for  $\hat{\theta}_k^{\text{bas}}$  and  $\hat{\theta}_k^{\text{bas},+}$ , as specified by Algorithm 2, reads

1002

1003

$$\hat{\theta}_{k+1}^{\text{bas}} = \hat{\theta}_k^{\text{bas}} - \eta m \nabla \hat{R}_U(\hat{\theta}_k^{\text{bas}}), \quad (48)$$

1004

1005

$$\hat{\theta}_{k+1}^{\text{val}} = \hat{\theta}_{k+1}^{\text{bas}} - \varepsilon \eta m_{\text{val}} \nabla \hat{R}_{\text{val}}(\hat{\theta}_{k+1}^{\text{bas}}). \quad (49)$$

1006

1007 Hence, we can rewrite

1008

1009

$$\phi_i^{\text{lin}} \varepsilon = -\frac{1}{L} \sum_{s=1}^L \langle \nabla \ell(\hat{\theta}_s^{\text{bas}}; \mathbf{x}_i), \hat{\theta}_s^{\text{val}} - \hat{\theta}_s^{\text{bas}} \rangle.$$

1010

1011 Using the assumptions  $\|\nabla^2 \ell(\hat{\theta}_s^{\text{bas}}, \mathbf{x}_i)\|_{\text{op}} \leq C_1$ ,  $\|\hat{R}_{\text{val}}(\hat{\theta}_k^{\text{bas}})\| \leq C_1$ , we obtain

1012

1013

$$|\phi_i(\varepsilon) - \phi_i^{\text{lin}} \varepsilon| \leq \frac{1}{L} \sum_{s=1}^L \left| \ell(\hat{\theta}_s^{\text{val}}; \mathbf{x}_i) - \ell(\hat{\theta}_s^{\text{bas}}; \mathbf{x}_i) - \langle \nabla \ell(\hat{\theta}_s^{\text{bas}}; \mathbf{x}_i), \hat{\theta}_s^{\text{val}} - \hat{\theta}_s^{\text{bas}} \rangle \right| \quad (50)$$

1014

1015

$$\leq \frac{C}{L} \sum_{s=1}^L \|\hat{\theta}_s^{\text{val}} - \hat{\theta}_s^{\text{bas}}\|^2 \leq C(\varepsilon \eta m_{\text{val}})^2. \quad (51)$$

1016

1017 The claim thus follows by recalling that  $\eta \leq C_\eta/m$ .

1018

1026 **G PROOF OF THEOREM 2**  
10271028 To lighten notation, we define  $\mathbf{r}_k := \nabla \widehat{R}_{\text{val}}(\hat{\boldsymbol{\theta}}_k^{\text{bas}})$  and  $\mathbf{v}_k(i) := \nabla \ell(\hat{\boldsymbol{\theta}}_k^{\text{bas}}; \mathbf{x}_i)$ .  
10291030 For any  $L, L_1 \in \mathbb{Z}$ , we have  
1031

$$\begin{aligned}\Upsilon_i^{\text{lin}}(L) &= \Upsilon_i^{\text{lin},0}(L) + \Upsilon_i^{\text{lin},1}(L) + \Upsilon_i^{\text{lin},2}(L) + \Upsilon_i^{\text{lin},3}(L), \\ \Upsilon_i^{\text{lin},0}(L) &:= \frac{\eta m_{\text{val}}}{L} \sum_{0 \leq t < s \leq L_0} \langle \mathbf{r}_{t+1}, \mathbf{M}_{s,t+1}^{\top} \mathbf{v}_s(i) \rangle, \\ \Upsilon_i^{\text{lin},1}(L) &:= \frac{\eta m_{\text{val}}}{L} \sum_{0 \leq t \leq L_0, L_0 < s \leq L} \langle \mathbf{r}_{t+1}, \mathbf{M}_{s,t+1}^{\top} \mathbf{v}_s(i) \rangle, \\ \Upsilon_i^{\text{lin},2}(L) &:= \frac{\eta m_{\text{val}}}{L} \sum_{L_0 < t < s \leq L_0: |s-t| \geq L_1} \langle \mathbf{r}_{t+1}, \mathbf{M}_{s,t+1}^{\top} \mathbf{v}_s(i) \rangle, \\ \Upsilon_i^{\text{lin},3}(L) &:= \frac{\eta m_{\text{val}}}{L} \sum_{L_0 < t < s \leq L_0: |s-t| < L_1} \langle \mathbf{r}_{t+1}, \mathbf{M}_{s,t+1}^{\top} \mathbf{v}_s(i) \rangle.\end{aligned}$$

1046 Since by continuity we have  $\lim_{k \rightarrow \infty} \nabla^2 \widehat{R}_U(\hat{\boldsymbol{\theta}}_k^{\text{bas}}) = \mathbf{Q}_{\infty}$ , for any  $\delta \in (0, 1/2)$ , we can choose  $L_0$   
1047 large enough so that  $(1 - \delta)\mathbf{Q}_{\infty} \preceq \nabla^2 \widehat{R}_U(\hat{\boldsymbol{\theta}}_k^{\text{bas}}) \preceq (1 + \delta)\mathbf{Q}_{\infty}$  for all  $k > L_0$ . In particular there  
1048 exists  $c_0 > 0$  (independent of  $\varepsilon$ ) such that  $\|\mathbf{H}_k\|_{\text{op}} \leq (1 - c_0 m \eta)$  for all  $k > L_0$ .  
10491050 Clearly  $|\Upsilon_i^{\text{lin},0}(L)| \leq C(L_0)/L \rightarrow 0$  as  $L \rightarrow \infty$ . Further  
1051

$$\begin{aligned}|\Upsilon_i^{\text{lin},1}(L)| &\leq \frac{C \eta m_{\text{val}}}{L} \sum_{0 \leq t \leq L_0, L_0 < s \leq L} \|\mathbf{M}_{s,t+1}\|_{\text{op}} \\ &\leq \frac{C \eta m_{\text{val}}}{L} \sum_{0 \leq t \leq L_0, L_0 < s \leq L} (1 - c_0 m \eta)^{s-t-1} \\ &\leq \frac{C \eta m_{\text{val}}}{L} \frac{L_0}{c_0 m \eta} \rightarrow 0.\end{aligned}$$

1061 Finally, by increasing  $L_0$ , we can ensure that, for  $k > L_0$ ,  $\|\mathbf{H}_k - \mathbf{H}_{\infty}\|_{\text{op}} \leq \delta$ ,  $\|\mathbf{r}_k - \mathbf{r}_{\infty}\| \leq \delta$ ,  
1062  $\|\mathbf{v}_k(i) - \mathbf{v}_{\infty}(i)\| \leq \delta$  (where  $\mathbf{H}_{\infty} = \mathbf{I} - \eta m \mathbf{Q}_{\infty}$  and  $\mathbf{r}_{\infty}, \mathbf{v}_{\infty}(i)$ ). Hence  
1063

1064  $|\langle \mathbf{r}_{t+1}, \mathbf{M}_{s,t+1}^{\top} \mathbf{v}_s(i) \rangle - \langle \mathbf{r}_{\infty}, \mathbf{H}_{\infty}^{s-t-1} \mathbf{v}_{\infty}(i) \rangle| \leq C|t-s+1|(1 - c_0 m \eta)^{s-t-1} \delta.$   
1065

1066 Therefore, letting  
1067

1068  $\tilde{\Upsilon}_i^{\text{lin},2}(L) := \frac{\eta m_{\text{val}}}{L} \sum_{L_0 < t < s \leq L} \langle \mathbf{r}_{\infty}, \mathbf{H}_{\infty}^{s-t-1} \mathbf{v}_{\infty}(i) \rangle, \quad (52)$   
1069

1070 we have  
1071

$$\begin{aligned}|\Upsilon_i^{\text{lin},2}(L) - \tilde{\Upsilon}_i^{\text{lin},2}(L)| &\leq \frac{\eta m_{\text{val}}}{L} \sum_{L_0 < t < s \leq L} |\langle \mathbf{r}_{t+1}, \mathbf{M}_{s,t+1}^{\top} \mathbf{v}_s(i) \rangle - \langle \mathbf{r}_{\infty}, \mathbf{H}_{\infty}^{s-t-1} \mathbf{v}_{\infty}(i) \rangle| \\ &\leq \frac{\eta m_{\text{val}}}{L} \sum_{L_0 < t < s \leq L} C|t-s+1|(1 - c_0 m \eta)^{s-t-1} \delta \\ &\leq \eta m_{\text{val}} \cdot \frac{1}{(c_0 m \eta)^2} \delta.\end{aligned}$$

1080 Finally, using again  $|\langle \mathbf{r}_\infty, \mathbf{H}_\infty^{s-t-1} \mathbf{v}_\infty(i) \rangle| \leq (1 - c_0 m \eta)^{s-t-1}$ , we have  
 1081

$$\begin{aligned} 1082 \lim_{L \rightarrow \infty} \tilde{\Upsilon}_i^{\text{lin}, 2}(L) &= \lim_{L \rightarrow \infty} \frac{\eta m_{\text{val}}}{L} \sum_{L_0 < t \leq L} \sum_{s=t+1}^{\infty} \langle \mathbf{r}_\infty, \mathbf{H}_\infty^{s-t-1} \mathbf{v}_\infty(i) \rangle \\ 1083 &= \eta m_{\text{val}} \sum_{k=0}^{\infty} \langle \mathbf{r}_\infty, \mathbf{H}_\infty^k \mathbf{v}_\infty(i) \rangle \\ 1084 &= \eta m_{\text{val}} \langle \mathbf{r}_\infty, (\mathbf{I} - \mathbf{H}_\infty)^{-1} \mathbf{v}_\infty(i) \rangle \\ 1085 &= \frac{m_{\text{val}}}{m} \langle \mathbf{r}_\infty, \mathbf{Q}_\infty^{-1} \mathbf{v}_\infty(i) \rangle. \\ 1086 \end{aligned}$$

1087 This finishes the proof of the part of Eq. (18) which concerns the limit of  $\Upsilon_i^{\text{lin}}$ . The calculation of  
 1088  $\lim_{L \rightarrow \infty} S_i^{\text{lin}}(L)$  is completely analogous and we omit it.  
 1089

## 1090 H PROOF OF THEOREM 3

1091 To simplify notations, we write  $y_j = y(\mathbf{x}_j)$  for the response variables and  $\psi_j = \psi(\mathbf{x}_j)$  for the  
 1092 feature vectors. Similarly, for the  $y_j^{\text{val}} = y(\mathbf{z}_j^{\text{val}})$ ,  $\psi(\mathbf{z}_j^{\text{val}}) = \psi_j^{\text{val}}$ .  
 1093

1094 With these notations, we have  $\mathbf{H}_k = \mathbf{H}$  independent of  $k$  and

$$1095 \nabla \ell(\hat{\boldsymbol{\theta}}; \mathbf{x}_i) = -(y_i - \langle \psi_i, \boldsymbol{\theta} \rangle) \psi_i, \quad (53)$$

$$1096 \nabla \hat{R}_{\text{val}}(\boldsymbol{\theta}) = -\frac{1}{m} \boldsymbol{\Psi}^T (\mathbf{y} - \boldsymbol{\Psi} \boldsymbol{\theta}), \quad (54)$$

$$1097 \mathbf{H} = \mathbf{I} - \eta \boldsymbol{\Psi}^T \boldsymbol{\Psi}. \quad (55)$$

1098 Hence,

$$1099 \Upsilon_i^{\text{lin}} = \frac{\eta m_{\text{val}}}{L} \sum_{0 \leq t < s \leq L} r_s(i) \langle \boldsymbol{\Psi} \mathbf{r}_{t+1}^{\text{val}}, \mathbf{H}^{s-t-1} \psi_i \rangle, \quad (56)$$

$$1100 \mathbf{r}_t^{\text{val}} := \mathbf{y}^{\text{val}} - \boldsymbol{\psi}^{\text{val}} \hat{\boldsymbol{\theta}}_{t+1}^{\text{bas}}, \quad r_s(i) := y_i - \langle \psi_i, \hat{\boldsymbol{\theta}}_s^{\text{bas}} \rangle \quad (57)$$

1101 Since  $\mathbf{P}_\Psi$  is the projector onto the null-space of  $\mathbf{H}$ , and by our choice of  $\eta$ , we have  $\mathbf{H} = \mathbf{P}_\Psi + \mathbf{H}_\perp$ ,  
 1102 where the row/column space of  $\mathbf{H}_\perp$  is orthogonal to the one of  $\mathbf{P}_\Psi$  and  $\|\mathbf{H}_\perp\|_{\text{op}} = (1 - c_\psi \eta) \in$   
 1103  $[0, 1]$ . As a consequence  $\|\mathbf{H}^{s-t-1} - \mathbf{P}_\Psi\|_{\text{op}} \leq (1 - c_\psi \eta)^{s-t-1}$ .  
 1104

1105 Define

$$1106 \tilde{\Upsilon}_i^{\text{lin}} := \frac{\eta m_{\text{val}}}{L} \sum_{0 \leq t < s \leq L} r_s(i) \langle \boldsymbol{\Psi} \mathbf{r}_{t+1}^{\text{val}}, \mathbf{P}_\Psi \psi_i \rangle. \quad (58)$$

1107 Then we have

$$\begin{aligned} 1108 \left| \frac{1}{L} \Upsilon_i^{\text{lin}} - \frac{1}{L} \tilde{\Upsilon}_i^{\text{lin}} \right| &\leq \frac{\eta m_{\text{val}}}{L^2} \sum_{0 \leq t < s \leq L} \left| r_s(i) \langle \boldsymbol{\Psi} \mathbf{r}_{t+1}^{\text{val}}, \mathbf{P}_\Psi \psi_i \rangle \right| \\ 1109 &\leq \frac{\eta m_{\text{val}}}{L^2} \sum_{0 \leq t < s \leq L} |r_s(i)| \|\boldsymbol{\Psi} \mathbf{r}_{t+1}^{\text{val}}\| \|\mathbf{H}^{s-t-1} - \mathbf{P}_\Psi\|_{\text{op}} |\psi_i| \\ 1110 &\stackrel{(a)}{\leq} C \frac{\eta m_{\text{val}}}{L^2} \sum_{0 \leq t < s \leq L} (1 - c_\psi \eta)^{s-t-1} \\ 1111 &\leq C \frac{\eta m_{\text{val}}}{L} \frac{1}{c_\psi \eta} \xrightarrow{L \rightarrow \infty} 0. \end{aligned}$$

1112 In (a), we used the fact that  $\lim_{t \rightarrow \infty} \hat{\boldsymbol{\theta}}_t^{\text{bas}} = \hat{\boldsymbol{\theta}}$  (Bartlett et al., 2021), and therefore  $|r_s(i)|$ ,  $\|\boldsymbol{\Psi} \mathbf{r}_{t+1}^{\text{val}}\|$   
 1113 remain bounded as  $s, t \rightarrow \infty$ .

1134 In view of the above,  $\lim_{L \rightarrow \infty} \Upsilon_i^{\text{lin}} / L = \lim_{L \rightarrow \infty} \tilde{\Upsilon}_i^{\text{lin}} / L$ . For the latter, we have  
 1135

$$\begin{aligned} 1136 \quad \lim_{L \rightarrow \infty} \frac{1}{L} \tilde{\Upsilon}_i^{\text{lin}} &= \lim_{L \rightarrow \infty} \frac{\eta m_{\text{val}}}{L^2} \sum_{0 \leq t < s \leq L} r_s(i) \langle \Psi \mathbf{r}_{t+1}^{\text{val}}, \mathbf{P}_{\Psi} \psi_i \rangle \\ 1137 \\ 1138 \quad &= \lim_{L \rightarrow \infty} \frac{\eta m_{\text{val}}}{L^2} \sum_{L_0 \leq t < s \leq L} r_s(i) \langle \Psi \mathbf{r}_{t+1}^{\text{val}}, \mathbf{P}_{\Psi} \psi_i \rangle \\ 1139 \\ 1140 \quad &= \lim_{L \rightarrow \infty} \frac{\eta m_{\text{val}}}{L^2} \sum_{L_0 \leq t < s \leq L} r(i) \langle \Psi \mathbf{r}^{\text{val}}, \mathbf{P}_{\Psi} \psi_i \rangle + \text{err}(L_0, L), \\ 1141 \\ 1142 \end{aligned}$$

1143 where  
 1144

$$1145 \quad |\text{err}(L_0, L)| \leq C \sup_{s \geq L_0} |r_s(i) - r(i)| + C \sup_{t \geq L_0} \|\mathbf{r}_t^{\text{val}} - \mathbf{r}_{t+1}^{\text{val}}\|. \quad (59) \\ 1146$$

1147 Since  $\lim_{t \rightarrow \infty} \hat{\theta}_t^{\text{bas}} = \hat{\theta}$ , we have  $\lim_{L_0 \rightarrow \infty} \limsup_{L \rightarrow \infty} \text{err}(L_0, L) = 0$ . Therefore,  
 1148

$$\begin{aligned} 1149 \quad \lim_{L \rightarrow \infty} \frac{1}{L} \tilde{\Upsilon}_i^{\text{lin}} &= \lim_{L_0 \rightarrow \infty} \lim_{L \rightarrow \infty} \frac{\eta m_{\text{val}}}{L^2} \sum_{L_0 \leq t < s \leq L} r(i) \langle \Psi \mathbf{r}^{\text{val}}, \mathbf{P}_{\Psi} \psi_i \rangle \\ 1150 \\ 1151 \quad &= \frac{1}{2} \eta m_{\text{val}} r(i) \langle \Psi \mathbf{r}^{\text{val}}, \mathbf{P}_{\Psi} \psi_i \rangle. \\ 1152 \\ 1153 \end{aligned}$$

1154 This proves the limit for  $\Upsilon_i^{\text{lin}}(L)$  in Eq. (19).  
 1155

1156 The limit of  $S_i^{\text{lin}}(L)$  is computed essentially by the same argument and we omit the derivation.  
 1157

## 1158 I LIMITATION

1159 The core idea of “train-on-validation” impacting training examples is general, but the specific scoring  
 1160 function  $F(\cdot)$  and aggregation strategy might need adaptation for different problem settings.  
 1161

1162 The SCORE+RANDOM selection strategy often outperformed SCORE-ONLY in our experiments,  
 1163 suggesting that diversity plays an important role beyond simply selecting the “most affected” ex-  
 1164 amples. While this is a practical improvement, it also indicates that our current scoring mechanism  
 1165 might not fully capture the optimal diversity or coverage needed for effective generalization. It will  
 1166 be interesting to explore more sophisticated diversity-aware scoring or selection mechanisms that  
 1167 explicitly balance our scoring methods with representation across the data space.  
 1168

1169 Although we mitigated bias toward shorter examples through length-based binning, a more refined  
 1170 length-normalization or task-specific weighting might further enhance the selection process. Fur-  
 1171 thermore, it will be interesting to see if the performance of our strategies further improves compared  
 1172 to random selection if the learning rate is also tuned for these strategies and not just for random  
 1173 selection.

1174 Finally, our theoretical analysis relies on stylized settings that are plausible for simple models but  
 1175 may not hold in many large-scale applications.  
 1176

## 1177 J MODELS AND DATASETS INFORMATION

### 1178 J.1 DATASET INFORMATION

- 1181 • Slim Orca:
  - 1182 – [Link](#)
  - 1183 – Citations-[Longpre et al. \(2023\)](#); [Mukherjee et al. \(2023\)](#); [Lian et al. \(2023\)](#)
  - 1184 – Licence: mit
- 1185 • Alpaca GPT-4:
  - 1186 – Paper:[Peng et al. \(2023\)](#)
  - 1187 – [Repository](#)

1188           – [Link](#)  
 1189           – Licence: cc-by-nc-4.0  
 1190        • Alpaca GPT-3.5:  
 1191           – Paper: [Taori et al. \(2023\)](#)  
 1192           – [Link](#)  
 1193           – Licence: cc-by-nc-4.0  
 1194        • Multinerd:  
 1195           – Paper: [Tedeschi & Navigli \(2022\)](#)  
 1196           – [Link](#)  
 1197           – Licence: cc-by-nc-sa-4.0  
 1198        • Ai4p:  
 1199           – [Link](#)  
 1200           – Licence: [link](#)  
 1201        • C4 dataset:  
 1202           – [Link](#)  
 1203           – Labeled for NER task using llms.  
 1204           – Licence: [terms of use](#)  
 1205        • Syn-Big:  
 1206           – Synthetically generated by us using llms.  
 1207           – Proprietary dataset

## 1212 J.2 PRETRAINED MODEL INFORMATION

1213        • Meta-Llama-3-8B [AI@Meta \(2024\)](#)  
 1214           – [Link](#)  
 1215           – License: llama3  
 1216        • xlm-roberta-base [Conneau et al. \(2019\)](#)  
 1217           – [Link](#)  
 1218           – License: mit

1221  
 1222  
 1223  
 1224  
 1225  
 1226  
 1227  
 1228  
 1229  
 1230  
 1231  
 1232  
 1233  
 1234  
 1235  
 1236  
 1237  
 1238  
 1239  
 1240  
 1241